Spatio-Temporal SIC-Based Slotted ALOHA with Multi-Antenna Reception

Yuhei Takahashi*, Daiki Fukui*, Guanghui Song†, Tomotaka Kimura*, Zilong Liu‡, and Jun Cheng*

Abstract—Previous studies on slotted ALOHA (SA) with temporal successive interference cancellation (SIC) and real-time feedback have primarily focused on single-antenna configurations under Rayleigh fading, offering limited analytical insights into multi-antenna systems with realistic fading conditions. To address this limitation, we develop an analytical framework for evaluating spatio-temporal SIC-based SA with multi-antenna reception over mixture Gamma fading channels. By applying the inclusion–exclusion principle to multi-antenna reception, we derive closed-form state-transition probabilities for the two-device case. These results enable exact computation of the average sum rate through a Markov-based formulation and facilitate the joint optimization of the transmission probability and code rate. The analytical results show excellent agreement with simulations, validating the proposed closed-form expressions and quantitatively demonstrating the performance gains achieved by multi-antenna reception.

Index Terms—Mixture Gamma distribution, multi-antenna reception, slotted ALOHA, successive interference cancellation

I. Introduction

Massive machine-type communication (mMTC) in the sixth generation (6G) is expected to be enabled by near-instant, ubiquitous wireless connectivity and to provide energy- and spectral-efficient connectivity to a large number of devices [1]. Among various approaches, random access (RA) schemes [2], [3], which evolved from slotted ALOHA (SA) [4], can efficiently support mMTC by allowing devices to transmit in an 'arrive-and-go' manner. In conventional SA, K_T devices randomly transmit their packets to an Access Point (AP) and collided packets are discarded (i.e., collision channel model). The AP broadcasts a *real-time* feedback (i.e., ACK) at the end of each slot. This real-time feedback ACK signal indicates decoding success or failure, and failed devices retransmit. In a system with K_T devices, the throughput of conventional SA is maximized when the transmission probability is set to $1/K_T$, yielding an asymptotic limit of $1/e$ [5], [6].

The collision channel model is often considered pessimistic. In practice, fading causes power variations among signals within a collision slot, which may allow the *capture effect* to occur when a sufficiently strong signal can be decoded

* Department of Intelligent Information Engineering and Sciences, Doshisha University, Kyoto, 610-0321, Japan
(e-mail: cyjk1101@mail4.doshisha.ac.jp; ctwk0108@mail4.doshisha.ac.jp; tomkimur@mail.doshisha.ac.jp; jcheng@ieee.org)
† The State Key Laboratory of Integrated Services Networks, Xidian University, Xi'an 710071, China
(e-mail: songguanghui@xidian.edu.cn)
‡ School of Computer Science and Electronic Engineering, University of Essex, Colchester, CO4 3SQ, UK
(e-mail: zilong.liu@essex.ac.uk)

[7]–[9]. For SA, the AP employs threshold-based decoding to recover the received packets within a slot. Successful decoding of certain packets at the AP may be possible provided that their signal-to-interference-plus-noise ratio (SINR) exceeds a decoding threshold [10]. Furthermore, *intra-slot* successive interference cancellation (SIC) can be exploited to enhance the decodability [11]. In [11], the probability $\Pr\{E_m^n\}$ was derived for generic fading models, denoting the event that among the n colliding packets, the first $m-1$ packets and the m-th (reference) packet are successfully decoded. This result enables throughput analysis. Moreover, in [12], Tegos *et al.* analyzed SA with intra-slot SIC, where devices transmit with different code rates. They derived closed-form expressions for the throughput over Rayleigh and Nakagami-m fading channels in the two-device collision scenario. Power control has also been investigated to improve the throughput of SA over Rayleigh fading [13], where each device randomly selects its transmit power based on its channel state information (CSI). A suboptimal discrete power distribution was derived for resolving two-device collisions with intra-slot SIC.

The aforementioned conventional SA schemes [4], [6], [7], [9]–[14] assume a single-antenna AP. In contrast, several studies have explored SA protocols under general spatial-diversity reception, including multi-antenna and multi-receiver settings. The throughput of the capture effect was first analyzed for a two-antenna AP under Rayleigh fading in [15], and was later extended to the case of an arbitrary number of antennas including log-normal shadowing in [16]. In these studies [15], [16], each antenna operates independently and attempts to decode the packet that has the highest signal-to-interference ratio (SIR) at that antenna among the simultaneously received signals. Owing to independent fading across antennas, the strongest signal may differ from one antenna to another, which allows multiple packets to be successfully received within the same slot. This configuration realizes a form of *non-cooperative* spatial diversity, where each receiving antenna independently captures a packet without cooperation among antennas. The capture probability at each antenna is assumed to be identical, and under the assumption of independent fading across antennas, the throughput corresponding to multiple colliding packets is derived based on the inclusion–exclusion principle.

Under random fading conditions, such as Rayleigh fading, obtaining closed-form solutions is intractable. Therefore, the *packet-erasure channel* model was employed for analytical simplicity in studying SA. In this model, a transmitted packet is considered erased if it encounters deep fading, thus categorizing it as an *on–off fading channel*. Using this simplified

model, the throughput of SA with multiple receivers was calculated [17], [18], highlighting that only singleton-packet slots can be decodable at each receiver and the receivers operate independently and without any cooperation. Moreover, the throughput analysis of spatial successive decoding among receivers was subsequently presented using a bipartite graph framework [19]. Furthermore, directional-antenna transmission used in [20] represents a practical embodiment of the packet-erasure (on–off) channel model, since packets falling outside the antenna beam are effectively "erased." Both analytical and simulation results demonstrate a clear performance advantage of cooperative multi-receiver decoding with SIC over non-cooperative decoding.

In parallel with spatial diversity, *temporal diversity* has been exploited to enhance throughput by randomly transmitting packets or their replicas into a subset of slots within a frame, a scheme known as irregular repetition slotted ALOHA (IRSA) [21]–[26]. The average asymptotic normalized throughput under intra- and inter-slot SIC was analyzed using the density evolution (DE) algorithm [27]. Moreover, the converse bound and the maximum a posteriori (MAP) decoding threshold for IRSA throughput were derived in [28]. Although these studies [27], [28] adopt a Rayleigh fading model rather than the simplified on–off model, they consider an AP with only a single antenna, which severely constrains the achievable spatial diversity.

Introducing the general spatial-diversity reception into IRSA leads to joint *spatio-temporal* SIC decoding schemes [29]. Because users are randomly located with respect to multiple base stations, each receiver experiences distinct large-scale attenuation; thus, a packet may be strong at one station but too weak—hence treated as "erased"—at another. This spatially varying packet-erasure behavior is exploited in [29] to enable cooperative spatio-temporal SIC. This analysis [29], however, still relies on the packet-erasure channel model, which does not capture the continuous nature of realistic fading. A probabilistic framework based on Poisson receivers has also been proposed for coded SA with multiple receivers [30]–[32]. In this framework, which includes IRSA as a special case, a Poisson receiver abstracts the packet-success probability under a Poisson offered load, while still modeling the wireless channel as a packet-erasure channel. Using the same packet-erasure model, the throughput of frameless slotted ALOHA, which is conceptually related to IRSA through its graph-based SIC decoding, was analyzed in [33]–[35].

In contrast to the above works based on the packet-erasure channel, Srivatsa *et al.* [36, Theorem 3] investigated IRSA under a Rayleigh fading channel, where the received signal amplitudes follow a continuous fading distribution rather than an on–off abstraction. Their model incorporates maximal-ratio combining (MRC) at a multi-antenna receiver, enabling spatial diversity by coherently combining the energy of all replicas of a packet across antennas. The combined signal-to-noise ratio (SNR) is then used within the intra-slot SIC process to recover packets that would otherwise be undecodable in a single-antenna setting. This demonstrates how spatial diversity and SIC can be integrated under realistic fading conditions. In [36, Theorem 3], the throughput achieved via MRC-assisted

reception and inter-slot SIC is characterized under the assumption of perfect CSI, providing a performance benchmark for the system. While spatial diversity is exploited through MRC to enhance the effective SNR of each packet replica, the decoding process does not perform inter-antenna SIC within a slot, and collision resolution relies solely on inter-slot SIC across replicas. A related study by Srivatsa *et al.* [37] investigates a Bayesian user-activity-detection (UAD) for IRSA and characterizes the resulting throughput when channel estimation and UAD errors are present in a Rayleigh fading, multi-antenna setting.

Unlike conventional SA, SA with multiple transmissions, such as IRSA [21], [27], [28], operates without real-time feedback. Consequently, IRSA faces two main challenges. 1) In a feedback-free context, redundant packets may be transmitted, resulting in reduced spectral and energy efficiency. 2) Since decoding can only begin once all device transmissions in a frame have been completed, such schemes may be unsuitable for delay-sensitive applications [23].

To fully exploit temporal diversity, conventional SA systems can be modified by storing the collided packets or the residual signal containing undecoded packets in a buffer for further inter-slot SIC processing [38], [39]. In Rayleigh fading channels, iterative decoding for two-device SA combining intra- and inter-slot SIC has been analyzed using a Markov process, where the code rate is constrained to be at least 1. The optimal solution was exhaustively searched for the maximum sum rate by simulations [39]. To the best of our knowledge, the potential of further enhancing such buffered systems through spatial diversity has not yet been explored.

Against the aforementioned background, we consider a K_T-device SA system in which an AP is equipped with L antenna elements to exploit spatial diversity. Devices transmit coded packets with transmission probability p and code rate R. In every slot, the AP leverages its multiple antennas to perform intra- and inter-antenna SICs, buffers residual signals for inter-slot SIC, and acknowledges successfully decoded devices. We refer to this setup a spatio-temporal SIC-based SA system with multi-antenna reception.

Our main contributions in this paper are as follows:

1) **Closed-form analysis:** We apply the inclusion–exclusion principle to the multi-antenna reception incorporating intra- and inter-slot SIC to derive closed-form expressions for event probabilities in two-device SA. Although the probability derivations initially require separating the code rate into $R \geq 1$ and $0 < R < 1$, we show that the final expressions can be unified for $R > 0$. This unification significantly simplifies the analysis of event probabilities and the sum rate. Moreover, the regime $0 < R < 1$ is particularly important for SA, since multi-device interference typically necessitates the use of low-rate channel codes together with low-order modulation, resulting in effective code rates below one in practical physical-layer scenarios [40], [41]. Thus, the generalization to $R > 0$ directly aligns with realistic operating conditions.

2) **Sum-rate optimization:** We formulate a sum-rate maximization problem for the two-device spatio-temporal

SIC-based SA with multi-antenna reception and derive the optimal solution by jointly optimizing the transmission probability and the code rate of packets. The analytical results quantitatively reveal the sum-rate gain enabled by multi-antenna reception within the spatio-temporal SIC framework.

3) **General fading model:** We adopt the mixture Gamma (MG) distribution to model the received SNR, enabling performance analysis under a broad class of fading channels. While the framework is general, we present numerical results for three representative cases: Rayleigh, Nakagami-m, and Rician.

The remainder of this paper is organized as follows. Section II introduces the preliminaries of the MG distribution. Section III derives closed-form expressions for the events occurring at a single antenna under two-packet reception. Section IV presents the spatio-temporal SIC-based SA scheme with multi-antenna reception. Section V then formulates explicit expressions for the event probabilities in a two-device SA system over general fading channels. Finally, numerical and simulation results are provided in Section VI, followed by conclusions in Section VII.

II. PRELIMINARY: MIXTURE GAMMA DISTRIBUTION

This section reviews the fundamentals of the MG distribution and its approximation for some fading channels.

A. Probability Density Function (PDF)

The MG model is a linear combination of Gamma distributions. By using an MG distribution approximation, the PDF of the received SNR γ between a device and an AP over a variety of fading channels can be expressed as [42, Eq. (1)]

$$p(\gamma) = \sum_{i=1}^{N} w_i f_i(\gamma) = \sum_{i=1}^{N} a_i \gamma^{b_i-1} e^{-c_i \gamma}, \quad \gamma > 0 \quad (1)$$

where N is the number of terms for the MG distribution approximation; a_i, b_i and c_i are the parameters of the i-th Gamma component. The expected value of each random variable (RV) γ is $\bar{\gamma} \triangleq \mathbb{E}(\gamma)$. $f_i(\gamma) = \frac{c_i^{b_i} \gamma^{b_i-1} e^{-c_i \gamma}}{\Gamma(b_i)}$ is a standard Gamma distribution, $\Gamma(\cdot)$ is the Gamma function, $w_i = \frac{a_i \Gamma(b_i)}{c_i^{b_i}}$ is the weight coefficient of the i-th Gamma component, satisfying $\sum_{i=1}^{N} w_i = 1$.

In our work, the MG parameters b_i ($i = 1, 2, \ldots, N$) are assumed to be positive integers as in the literature. For the PDF of (1), it follows that

$$\int_0^{\infty} p(\gamma_j) \mathrm{d}\gamma_j = \sum_{i=1}^{N} a_i c_i^{-b_i} (b_i - 1)! = \sum_{i=1}^{N} d_i = 1$$

where, for compact notation, $d_i \triangleq a_i c_i^{-b_i} (b_i - 1)!$.

To integrate the MG distribution's PDF, it is necessary to evaluate the lower and upper incomplete Gamma functions as series expansions [43, Eq. 8.352.1] [43, Eq. 8.352.4], considering m as a positive integer.

$$\gamma(m, x) \triangleq \int_0^x t^{m-1} e^{-t} \mathrm{d}t = (m-1)!\left(1 - e^{-x} \sum_{k=0}^{m-1} \frac{x^k}{k!}\right). \quad (2)$$

$$\Gamma(m, x) \triangleq \int_x^{\infty} t^{m-1} e^{-t} \mathrm{d}t = (m-1)! e^{-x} \sum_{k=0}^{m-1} \frac{x^k}{k!}. \quad (3)$$

In addition, the (complete) Gamma function defined below is related to the factorial by [43, Eqs. (8.310.1) and (8.321.1)]

$$\Gamma(m) \triangleq \int_0^{\infty} t^{m-1} e^{-t} \mathrm{d}t = (m-1)!. \quad (4)$$

B. Mixture Gamma Distribution of Typical Fading Channels

In general, a fading model describes the distribution of the channel fading amplitude $|h|$. For example, Nakagami-m, Rayleigh, and Rician fading channels indicate that the distribution of the fading amplitude follows Nakagami-m, Rayleigh, and Rician distributions, respectively.

Since the received SNR is proportional to the squared amplitude of the received signal, it is known that if the fading amplitude follows a Rayleigh distribution (Nakagami-m distribution), then the received SNR follows an exponential distribution (Gamma distribution). Similarly, the Nakagami-Lognormal (NL) channel [44], [45] follows a Gamma-lognormal (GL) distribution [44], while other fading models such as the Generalized-K (K_G) [46], $\eta - \mu$ [47], Nakagami-q (Hoyt) [44], and $\kappa - \mu$ [47] channels follow their respective distributions.

For the rest of this section, we briefly describe Rician fading as an example of an MG distribution approximation. The corresponding SNR distribution of the Rician channel model is given as [44]

$$p_{\mathrm{R}}(\gamma) = \frac{(1+K)e^{-K}}{\bar{\gamma}} e^{-\frac{(1+K)}{\bar{\gamma}}\gamma} I_0\left(\sqrt{\frac{K(1+K)}{\bar{\gamma}}\gamma}\right), \gamma > 0 \quad (5)$$

where $K(\geqq 0)$ denotes the fading parameter, also known as the Rician factor. Additionally, $I_0(\cdot)$ is the zeroth-order modified Bessel function of the first kind, which can be computed as [44]

$$I_0(x) = \sum_{i=0}^{\infty} \frac{1}{(i!)^2} \left(\frac{x}{2}\right)^{2i}.$$

This function introduces mathematical complexity, making it difficult to obtain exact closed-form expressions, such as integrating in terms of the SNR γ.

The required accuracy to approximate the exact $p_{\mathrm{R}}(\gamma)$ can be achieved by summing a finite number of terms N in (1). By matching the PDF in (5), the parameters of the MG distribution can be evaluated as [42]

$$a_i = \frac{\theta_i}{\sum_{j=1}^{N} \theta_j \Gamma(b_j) c_j^{-b_j}}, \quad b_i = i, \quad c_i = \frac{1+K}{\bar{\gamma}},$$

$$\theta_i = \frac{1+K}{e^K[(i-1)!]^2 \bar{\gamma}} \left(\frac{K(1+K)}{\bar{\gamma}}\right)^{i-1}. \quad (6)$$

These parameters for the Rician channel model, as well as those for Rayleigh, Nakagami-m models, are provided in Table I [42]. As the MG accurately mirrors SNR distributions across multiple multipath fading models by adjusting its parameters as detailed in [48, Table II], our study retains its validity for the models outlined there.

TABLE I
PARAMETERS OF A MIXTURE GAMMA DISTRIBUTION
FOR DIFFERENT CHANNEL MODELS

Fading Model	Parameters of MG distribution
Rayleigh	$N = 1$, $a_1 = \frac{1}{\bar{\gamma}}$, $b_1 = 1$, $c_1 = \frac{1}{\bar{\gamma}}$
Nakagami-m	$N = 1$, $a_1 = \frac{m^m}{\Gamma(m)\bar{\gamma}^m}$, $b_1 = m$, $c_1 = \frac{m}{\bar{\gamma}}$
Rician	$N = 20$, (6)

TABLE II
EVENTS OCCURRING AT A SINGLE ANTENNA, WHERE P1 (P2) IS THE
PACKET SENT BY DEVICE 1 (2). (DEC: DECODABLE, UND:
UNDECODABLE, PD: POTENTIAL DECODABLE)

region	event		region	event
A, Ǎ	P1 and P2: Dec		D	P1: PD, P2: Und and not PD
B	P1: Dec, P2: Und and not PD		Ď	P1: Und and not PD, P2: PD
B̌	P1: Und and not PD, P2: Dec		E, Ě	P1 and P2: Und and not PD
C, Č	P1 and P2: PD			

III. PROBABILITIES IN TWO-COLLISION
(SINGLE-ANTENNA CASE)

In this section, we derive closed-form probability expressions for two packets being received in distinct SNR regions. These expressions will be used for computation of event probabilities in Section V.

A. Intra-Slot SIC

We consider a two-device fading channel with a single-antenna reception, where the received signal at a slot is given by $\boldsymbol{y} = \sum_{k=1}^{2} h_k \boldsymbol{x}_k + \boldsymbol{z}$. In this context, the device k is active and has accessed the slot. The vector $\boldsymbol{x}_k \in \mathcal{C}$ represents its codeword (or packet) of code $\mathcal{C}$, having length n and transmitted at rate R, where R denotes the information-theoretic transmission rate (spectral efficiency), measured in bits per channel use. In practice, such a rate, particularly when $R > 1$, can be realized by combining a channel code with higher–order modulation, although no specific coding scheme is assumed in this paper. Vector $\boldsymbol{z} \sim \mathcal{CN}(\boldsymbol{0}, \sigma^2 I)$ is an additive, circularly symmetric complex Gaussian (CSCG) noise with mean $\boldsymbol{0}$ and diagonal covariance matrix $\sigma^2 I$ with noise power σ^2 and identity matrix I. The channel coefficient h_k signifies the fading of the channel from the active device k to the AP during the slot, and it is kept constant for the duration of a slot and varies independently in the next slot. Every device is subjected to the identical power limitation $\|\boldsymbol{x}_k\|^2/n \leq P$, and the SNR of the signal received from the active device k is given by $\gamma_k = P|h_k|^2/\sigma^2$.

The channel coefficients are independent and identically distributed (i.i.d.) [39]. The random variable (RV) $|h_k|$ can be different kinds of fading channels, as shown in Table I. PDFs of their SNRs γ_k can be uniformly and approximately expressed by an MG distribution (1) [42], [48].

We employ threshold-based decoding [27], where the packet (codeword) $\boldsymbol{x}_k$ is successfully decoded if the SINR η_k exceeds the decoding threshold η_0, i.e.,

$$\Pr\{\text{packet } \boldsymbol{x}_k \text{ decoded}\} = \begin{cases} 1, & \eta_k > \eta_0, \\ 0, & \eta_k \leq \eta_0, \end{cases} \quad (7)$$

where the threshold for the SNR satisfies $R = \log_2(1 + \eta_0)$ for code rate R [49].

We outline the decoding process. Without loss of generality, we assume $\gamma_1 > \gamma_2$. In the first step, the SINR in the received signal $\boldsymbol{y}$ is

$$\eta_1 \triangleq \frac{P|h_1|^2}{\sigma^2 + P|h_2|^2} = \frac{\gamma_1}{1 + \gamma_2}.$$

Packet $\boldsymbol{x}_1$ will be successfully decoded if $\eta_1 > \eta_0$, and otherwise SIC will stop. We remove $h_1\boldsymbol{x}_1$ from $\boldsymbol{y}$ if the decoding is successful. In the second step, the SINR is

$$\eta_2 \triangleq P|h_2|^2/\sigma^2 = \gamma_2.$$

If $\eta_2 > \eta_0$, packet $\boldsymbol{x}_2$ in the slot is successfully decoded.

The decoding process described is termed *intra-slot SIC*. Note that the AP is assumed to have full CSI. In practice, obtaining full CSI is challenging due to fading and noise. However, for the sake of simplicity, we assume perfect CSI in this paper. The impact of CSI estimation errors is left for future work.

Packets within a slot are sorted into decodable or undecodable types in intra-slot SIC. An undecodable packet $\boldsymbol{x}_k$ with SNR above η_0, i.e., $\gamma_k > \eta_0$, is termed a *potentially decodable (PD)* packet [39], because it can be decoded upon removing the interfering packet $\boldsymbol{x}_{j\neq k}$ from signal $\boldsymbol{y}$.

At this point, we summarize the possible events at a single-antenna reception for the packets sent from device 1 and device 2, as shown in Table II.

Before deriving closed-form expressions for the probability of two packets being received in distinct SNR regions, we define $\Gamma = \{(\gamma_1, \gamma_2)|\gamma_1 \in \Gamma_1, \gamma_2 \in \Gamma_2\}$ as a probability region, with $\Gamma_1, \Gamma_2 \subseteq \mathcal{R}^+$ being subsets of the non-negative real numbers $\mathcal{R}^+$.

For the two independent RVs γ_1 and γ_2, the probability of being in region Γ is given by

$$P_\Gamma = \Pr\{(\gamma_1, \gamma_2)|\gamma_1 \in \Gamma_1, \gamma_2 \in \Gamma_2\} = \int_{\Gamma_2} p(\gamma_2) \int_{\Gamma_1} p(\gamma_1) \mathrm{d}\gamma_1 \mathrm{d}\gamma_2.$$

The probability expressions are divided into two cases: $R \geq 1$ and $R < 1$, as detailed below.

B. Closed-Form Expressions of Probabilities ($R \geq 1$)

In the case of $R \geq 1$, Fig. 1 illustrates the practical regions A to E ($\gamma_1 > \gamma_2$) along with their symmetric counterparts Ǎ to Ě ($\gamma_1 < \gamma_2$). The events listed in Table II are defined.

For $\gamma_1 > \gamma_2$, the probabilities for regions A to E are:

$$P_\mathsf{A} = \Pr\{\mathsf{A} : (\gamma_1, \gamma_2)|\gamma_1 > \eta_0(1 + \gamma_2), \gamma_2 > \eta_0\} \quad (8a)$$

$$P_\mathsf{B} = \Pr\{\mathsf{B} : (\gamma_1, \gamma_2)|\gamma_1 > \eta_0(1 + \gamma_2), \gamma_2 \leq \eta_0\} \quad (8b)$$

$$P_\mathsf{C} = \Pr\{\mathsf{C} : (\gamma_1, \gamma_2)|\gamma_2 < \gamma_1 \leq \eta_0(1 + \gamma_2), \gamma_2 > \eta_0\} \quad (8c)$$

$$P_\mathsf{D} = \Pr\{\mathsf{D} : (\gamma_1, \gamma_2)|\eta_0 < \gamma_1 \leq \eta_0(1 + \gamma_2), \gamma_2 \leq \eta_0\} \quad (8d)$$

$$P_\mathsf{E} = \Pr\{\mathsf{E} : (\gamma_1, \gamma_2)|\gamma_2 < \gamma_1 \leq \eta_0, \gamma_2 \leq \eta_0\}. \quad (8e)$$

For $\gamma_1 < \gamma_2$, the probabilities for regions Ǎ to Ě are defined analogously. In Appendix I-A, we derive the closed-form expressions for probabilities P_A through P_E while excluding $P_\mathsf{Ǎ}$ and $P_\mathsf{Ě}$ due to symmetry.
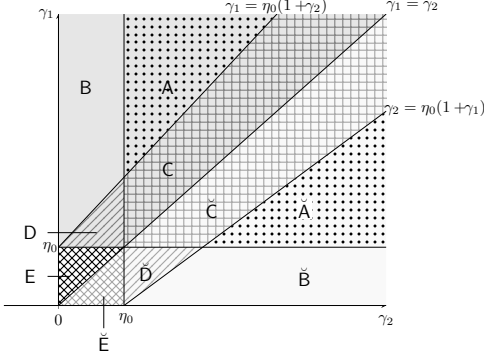
Fig. 1. The SIC feasible region in a two-device SA under $R \geq 1$.

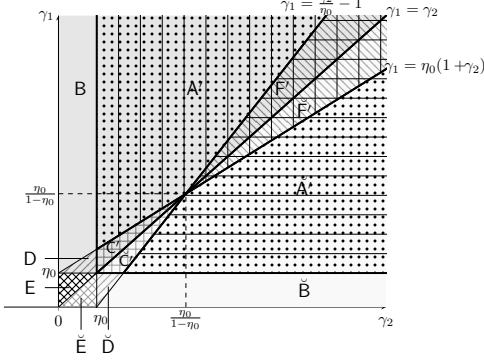Fig. 2. The SIC feasible region in a two-device SA under $0 < R < 1$. Vertical lines illustrate the region $(\mathsf{A}' \cup \mathsf{F}' \cup \check{\mathsf{F}}')$, while horizontal lines represent the region $(\check{\mathsf{A}}' \cup \mathsf{F}' \cup \check{\mathsf{F}}')$.

C. Closed-Form Expressions of Probabilities ($0 < R < 1$)

In the case of $R < 1$, the decoding threshold η_0 is less than 1, i.e., $\eta_0 < 1$. This implies that the two lines $\gamma_1 = \gamma_2$ and $\gamma_1 = \eta_0(1 + \gamma_2)$ (or $\gamma_2 = \eta_0(1 + \gamma_1)$) intersect at a point denoted by $(\frac{\eta_0}{1-\eta_0}, \frac{\eta_0}{1-\eta_0})$ (see Fig. 2), where $\frac{\eta_0}{1-\eta_0}$ is a unique solution to equation $\gamma_1 = \eta_0(1 + \gamma_1)$ (or $\gamma_2 = \eta_0(1 + \gamma_2)$).

This implies that the probability that both packets are decodable over the entire $\gamma_1 - \gamma_2$ plane is given by

$$\Pr\left\{\mathsf{A}' \cup \check{\mathsf{A}}' \cup \mathsf{F}' \cup \check{\mathsf{F}}'\right\} = (P_{\mathsf{A}' \cup \mathsf{F}' \cup \check{\mathsf{F}}'} - P_{\check{\mathsf{F}}'}) + (P_{\check{\mathsf{A}}' \cup \mathsf{F}' \cup \check{\mathsf{F}}'} - P_{\mathsf{F}'}).$$

Note that the ranges of the double integral used to compute $P_{\mathsf{A}' \cup \mathsf{F}' \cup \check{\mathsf{F}}'}$ are the same as those in (8a).

In order to integrate both cases of R, as in the case of $R \geq 1$, we give the probabilities for the case $\gamma_1 > \gamma_2$:

$$
\begin{aligned}
P_{(\mathsf{A}' \cup \mathsf{F}')} &= P_{\mathsf{A}' \cup \mathsf{F}' \cup \check{\mathsf{F}}'} - P_{\check{\mathsf{F}}'} \\
&= \Pr\left\{(\gamma_1, \gamma_2) | \gamma_1 > \eta_0(1 + \gamma_2), \gamma_2 > \eta_0\right\} \\
&\quad - \Pr\left\{(\gamma_1, \gamma_2) | \eta_0(1+\gamma_2) < \gamma_1 < \gamma_2, \gamma_2 > \frac{\eta_0}{1-\eta_0}\right\}, \\
P_{\mathsf{C}'} &= \Pr\left\{(\gamma_1, \gamma_2) | \gamma_2 < \gamma_1 < \eta_0(1+\gamma_2), \eta_0 < \gamma_2 < \frac{\eta_0}{1-\eta_0}\right\}.
\end{aligned}
$$

The probabilities for region $(\check{\mathsf{A}}' \cup \check{\mathsf{F}}')$ and $\check{\mathsf{C}}'$ ($\gamma_1 < \gamma_2$) can be derived in a similar manner, and are omitted for brevity. We derive the closed-form expressions of $P_{(\mathsf{A}' \cup \mathsf{F}')}$ and $P_{\mathsf{C}'}$ in

Appendix I-B. Note that the closed-form expressions of P_{B}, P_{D}, and P_{E} remain invariant with respect to R.

Since both $P_{(\mathsf{A}' \cup \mathsf{F}')}$ and P_{A} represent the probability that two packets are successfully decoded, we adopt the unified notation P_{A} and extend it to the regime $0 < R < 1$. In this range, P_{A} follows the expression originally derived for $P_{(\mathsf{A}' \cup \mathsf{F}')}$, whereas for $R \geq 1$, it follows the expression previously denoted by P_{A}. Likewise, the probability P_{C} is extended to $0 < R < 1$ by employing its counterpart $P_{\mathsf{C}'}$ defined for this regime.

Before concluding this section, it is worth noting that although the above derivations are separated into two cases ($R \geq 1$ and $0 < R < 1$), a key outcome is that the final expressions can be unified into $R > 0$, with only some intermediate formulas retaining the two-case form. An advantage of this result is that it allows the derivation of event probabilities and, consequently, the sum rate of the two-device SA (Section V), under the general condition $R > 0$ without distinguishing between the two cases. While many SA studies focus solely on the $R \geq 1$ regime (e.g., [27], [28], [39], [50]), practical systems often operate with $0 < R < 1$ due to multi-device interference and the need for low-rate channel coding together with low-order modulation [41]. Nevertheless, our unified result ensures that the derived expressions remain valid for all $R > 0$.

IV. SIC-Based SA with Multi-Antenna Reception

In this section, we describe the spatio-temporal SIC-based SA with real-time feedback and multi-antenna reception, along with an analysis of their asymptotic performance using a Markov process. Our work is an extension of a single antenna reception over the Rayleigh fading channel [39] to a *multi-antenna* reception over a more general channel whose SNR is modeled by the MG distribution.

A. Random Uplink Transmission and Re-transmission

We examine the SA system comprising one L-antenna AP and K_{T} single-antenna devices, wherein the devices aim to deliver messages to the AP using an SA protocol, as shown in Fig. 3. Let $\mathcal{K}$ and $\mathcal{L}$ denote the set of active devices and the set of antenna indices, respectively, where $|\mathcal{K}| = K_a (\leq K_{\mathsf{T}})$, $|\mathcal{L}| = L$. The antennas in the AP are spaced sufficiently far apart to ensure independent fading values, with the required spacing varying from $\lambda/2$ to approximately 10λ, where λ represents the wavelength [51].

The system employs a shared code $\mathcal{C}$ with code rate R. This encoder could be a combination of a channel encoder and a modulator. We assume that each device possesses an individual message stream. Each message is encoded into a codeword, known as a packet, using code $\mathcal{C}$. Following the SA protocol, the complete transmission period is segmented into time slots, whereby each slot's duration is designed to accommodate the transmission of a single packet. During time slot t, each device transmits or re-transmits its packet to the AP with transmission probability p and at power P. Once a packet is transmitted successfully, the device refreshes its message
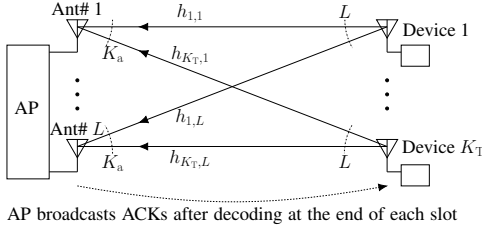
Fig. 3. A K_T-device SA system, where at slot t, K_a devices are active and send their packets to the AP equipped with L antenna elements. The AP processes the signals received during the current slot and any residual signals from past slots to recover the transmitted packets.

stream in preparation to send a new packet. By assumption, the devices are synchronized in terms of symbols and slots.

In the receiver, the AP iteratively decodes from the L received signals at slot t and residual signals from past slots, feeding real-time confirmation messages, i.e., ACKs, back to the devices at the end of each slot.

B. Spatio-Temporal SIC Decoding

Consider a generic slot, e.g., slot t, at some point during decoding. For the sake of concise notation, we omit the time index t in this subsection. Assuming K_a $(\leq K_\mathrm{T})$ devices are active and transmit their packets in the slot, the resultant L superimposed signals, one per antenna, within the slot are

$$\boldsymbol{y}_i = \sum\nolimits_{k \in \mathcal{K}} h_{k,i} \boldsymbol{x}_k + \boldsymbol{z}_i, \quad i = 1, 2, \ldots, L. \tag{9}$$

Here, device k is active and accesses the current slot. Vectors $\boldsymbol{x}_k$ and $\boldsymbol{z}_i$ correspond to those detailed in Section III-A. The channel coefficient $h_{k,i}$ expresses the fading of the channel from the active device k to Ant# i of the AP during the slot, and it is kept constant for one slot and then changed independently for the next slot. The SNR of the signal received from the active device k at Ant# i is expressed as $\gamma_{ki} = P|h_{k,i}|^2/\sigma^2$. The PDF of SNR γ_{ki} can be uniformly and approximately expressed by an MG distribution in (1).

The following spatio-temporal SIC decoding process, influenced by transmission and spatial diversities, involves a complex iterative procedure integrating both intra- and inter-slot, as well as intra- and inter-antenna SICs (see Algorithm 1).

1) Intra-Slot SIC: In the AP, decoding within a slot involves an iterative process alternating between intra-antenna and inter-antenna SICs. It is assumed that the AP has full awareness of the CSI and the number of packet collisions.

a) Intra-Antenna SIC: At Ant# i, the SINR of the packet from device k, assuming $\gamma_{1i} > \gamma_{2i} > \cdots > \gamma_{K_\mathrm{a}i}$, can be calculated as

$$\eta_{k,i} \triangleq \frac{P|h_{k,i}|^2}{\sigma^2 + \sum_{u=k+1}^{K_\mathrm{a}} P|h_{u,i}|^2} = \frac{\gamma_{ki}}{1 + \sum_{u=k+1}^{K_\mathrm{a}} \gamma_{ui}}. \tag{10}$$

Following threshold-based decoding, the packet $\boldsymbol{x}_k$ is successfully decoded if the SINR $\eta_{k,i}$ exceeds a certain threshold η_0 (see (7)). Upon successful decoding, the packet is removed from the received signal $\boldsymbol{y}_i$. Subsequent decoding proceeds with the interference-removed signal. This iterative process is termed *intra-antenna SIC*.

b) Inter-Antenna SIC: The previously described intra-antenna SIC process enables the successful decoding of packets. These decoded packets are then canceled from the signals of other antennas within the same slot. This procedure is referred to as *inter-antenna SIC*.

The above two processes are repeated across all antenna elements until no further decoding is possible for any packets on any antenna element. This iterative decoding procedure is referred to as *intra-slot SIC* due to its execution within a slot.

Due to random fading, the complete recovery of all K_a packets cannot be ensured within a slot. The slot t is m-*recovery* if the AP can successively recover m $(\leq K_\mathrm{a})$ packets from $\boldsymbol{y}_i$, $i = 1, 2, \ldots, L$, with the intra-slot SIC. After removing the recovered packets from $\boldsymbol{y}_i$, any residual signals, each per antenna, are stored into a residual buffer for further processing.

2) Inter-Slot SIC: Following the intra-slot SIC at slot t, if a recovered packet in the slot is identified as a re-transmission, its replicas will be canceled from the associated residual signal(s) at earlier slots j $(< t)$ within the residual buffer. This enables further intra-slot SICs on these signals.

The above process is repeated until decoding is no longer possible for any packets in the buffer. Upon successful recovery of packets, at the end of slot t, the AP sends ACKs to the respective devices. The overall iterative decoding process, integrating both intra- and inter-slot as well as intra- and inter-antenna SICs, is summarized in Algorithm 1, and an example is illustrated in Fig. 4, where a two-antenna AP decodes two packets within a slot.

C. Markov Process of Two-Device SA with Multi-Antenna

This subsection examines the modeling of the SIC-based two-device SA with real-time feedback and multi-antenna reception as a Markov process, specifically constraining the number of devices to $K_\mathrm{T} = 2$.

Before describing the states of the residual buffer, we extend the definition of a *potentially-decodable* (*PD*) packet

---

Algorithm 1 Spatio-Temporal SIC Decoding

1: **Initialize:** Let t be the index of the current slot
2: **if** any packets at slot t are m-recovery with $m > 0$ **then**
3:     **for** Ant# $i = 1$ to L **do**
4:         *Intra-antenna SIC* in Ant# i.
5:         *Inter-antenna SIC* in slot t.
6:     **end for**
7:     *Inter-slot SIC* (if retransmitted packets are recovered).
8:     Store residual signals, each per antenna, into the buffer.
9:     **while** any buffer slot $t'(< t)$ is m'-recovery $(m' > 0)$ **do**
10:         **for** Ant# $i = 1$ to L **do**
11:             *Intra-antenna SIC* in Ant# i.
12:             *Inter-antenna SIC* in slot t'.
13:         **end for**
14:         *Inter-slot SIC* (if retransmitted packets are recovered).
15:     **end while**
16:     ACK feedback for each recovered packet.
17: **else**
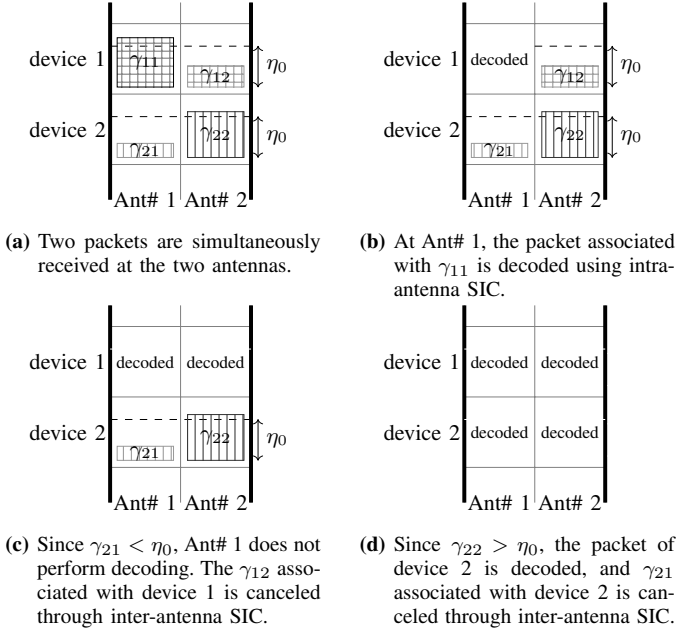18:   Store received signals, each per antenna, into the buffer.
19: **end if**

(a) Two packets are simultaneously received at the two antennas.

(b) At Ant# 1, the packet associated with γ_{11} is decoded using intra-antenna SIC.

(c) Since $\gamma_{21} < \eta_0$, Ant# 1 does not perform decoding. The γ_{12} associated with device 1 is canceled through inter-antenna SIC.

(d) Since $\gamma_{22} > \eta_0$, the packet of device 2 is decoded, and γ_{21} associated with device 2 is canceled through inter-antenna SIC.

Fig. 4. Example of intra- and inter-antenna SIC decoding within a two-packet slot. The AP is equipped with $L = 2$ antennas.

Fig. 5. State-transition diagram of the Markov process for the two-device case [39].

[39], previously introduced for the single-antenna case in Section III-A, to the multi-antenna setting. In the context of residual signals, an unrecovered packet $\boldsymbol{x}_k$ qualifies as *PD*, if there exists at least one antenna element, i.e., Ant# i, such that its SNR exceeds the decoding threshold η_0. In a two-collision scenario, each of the L residual signals can contain zero, one, or two *PD* packets. In contrast, for a single-packet slot (one-collision), storing an undecodable packet in the buffer is redundant, hence no *PD* packets are present. The buffer is said to contain q ($q = 2, 1, 0$) PD packets when q is the highest number of PD packets found in the L residual signals.

The decoding process between intra- and inter-slot SIC can be modeled as a Markov process, whose state-transition diagram is shown in Fig. 5. The state set of the two-device residual signal buffer is defined as $\mathcal{S} = \{S_0, S_1, S_2\}$. State S_0 indicates that no PD packet exists in the buffer, and state S_1 (S_2) indicates that one (two) *PD* packets exist(s).

Let $\Pr\{s_t, d_t | s_{t-1}\}$ be the probability of a state transition from s_{t-1} to s_t and let d_t packets be recovered along with this state transition. A state-transition probability polynomial is defined as $p_{s_{t-1}, s_t}(x) \triangleq \sum_{d=0}^{2} \Pr\{s_t, d_t = d | s_{t-1}\} x^d$ [38]. A state transition is triggered by decoding in the current slot t. The events that occur in the decoding of slot t are described in Table III.

Let us explain the state transitions, for example, from

$s_{t-1} = S_0$ to $s_t = S_0$. During the decoding of slot t, six scenarios can lead to this transition. First, if two devices are inactive (event E_0^0) and the buffer is empty, there is no residual signal in the slot t. If all packets are decodable (event E_1^1 and E_2^2), the buffer is updated to $s_t = S_0$. Similarly, when one of the two packets is successfully decoded while the other is undecodable and not a *PD* packet (event E_1^2), the buffer is likewise updated to $s_t = S_0$. When a packet is undecodable in a one-collision and is ineligible as a *PD* packet (event E_0^1), the packet is not stored in the buffer, resulting in the buffer state transitioning to $s_t = S_0$. Finally, when two packets are undecodable and invalid as *PD* packets (event E_0^{Col}), the buffer state is transformed to $s_t = S_0$. The probabilities for these transitions are given by

$$\Pr\{s_t = S_0, d_t = 0 | s_{t-1} = S_0\} = P\{E_0^0\} + P\{E_0^1\} + P\{E_0^{\mathrm{Col}}\}$$
$$\Pr\{s_t = S_0, d_t = 1 | s_{t-1} = S_0\} = P\{E_0^1\} + P\{E_1^2\}$$
$$\Pr\{s_t = S_0, d_t = 2 | s_{t-1} = S_0\} = P\{E_2^2\}.$$

The polynomial representing the state-transition probability is

$$p_{s_{t-1}=S_0, s_t=S_0}(x) = P\{E_0^0\} + P\{E_0^1\}x + P\{E_0^1\}$$
$$+ P\{E_2^2\}x^2 + P\{E_1^2\}x + P\{E_0^{\mathrm{Col}}\}$$

The state-transition polynomial matrix is given in (11) [39].

Remark 1. *The state-transition diagram of Fig. 5 remains consistent across various fading models, as the decoding process is independent of variations in the fading models. Moreover, for multi-antenna reception, the proposed inter-antenna SIC is integrated as a component of the intra-slot SIC process, ensuring that the state-transition diagram is preserved within this Markov model. It is noteworthy that, despite the diagram being consistent, calculating the transition probabilities presents a challenge, particularly when considering multi-antenna reception with a general fading model.* □

The first-order derivative $\mathrm{d}p_{s', s}(x)/\mathrm{d}x$ evaluated at $x = 1$ indicates the expected number of packets retrieved during the transition from state s' to state s. Consequently, matrix $P'(x = 1) = \mathrm{d}P(x)/\mathrm{d}x|_{x=1}$, which measures the number of packets during transition, is then

$$P'(1) = \begin{pmatrix} P\{E_1^1\} + P\{E_1^2\} + 2P\{E_2^2\} & 0 & 0 \\ 2P\{E_{\mathrm{nop}}^{\mathrm{rec}}\} + P\{E_{\mathrm{pot}}^{\mathrm{rec}}\} & 0 & 0 \\ 2P\{E_1^1\} + 2P\{E_2^2\} + 2P\{E_1^2\} & 0 & 0 \end{pmatrix}. \quad (12)$$

Let a stationary distribution of the Markov process be $\boldsymbol{w} = (w_0, w_1, w_2)^{\mathrm{T}}$, such that $\boldsymbol{w}^{\mathrm{T}} P(x = 1) = \boldsymbol{w}^{\mathrm{T}}$ and $\boldsymbol{w}^{\mathrm{T}} \mathbf{1} = 1$, where $\mathbf{1} = (1, 1, 1)^{\mathrm{T}}$. The normalized throughput of the two-device SA with SICs and feedback, as $t \to \infty$, is given by

$$T(p, R, \bar{\gamma}, L) = \boldsymbol{w}^{\mathrm{T}} P'(1) \mathbf{1} \text{ packets/slot} \quad (13)$$

which represents the average number of packets successfully decoded per time slot with L antennas.

Furthermore, the sum rate is defined as

$$R_{\mathrm{s}} \triangleq R \cdot T(p, R, \bar{\gamma}, L) \text{ bits/channel use} \quad (14)$$

which represents the expected amount of information recovered from each received symbol.

$$P(x) = \begin{pmatrix} P\{E_0^0\} + P\{E_1^1\}x + P\{E_0^1\} + P\{E_2^2\}x^2 + P\{E_1^2\}x + P\{E_0^{\mathrm{Col}}\} & P\{E_1^{\mathrm{Col}}\} & P\{E_2^{\mathrm{Col}}\} \\ P\{E_{\mathrm{nop}}^{\mathrm{rec}}\}x^2 + P\{E_{\mathrm{pot}}^{\mathrm{rec}}\}x & P\{E_0^0\} + P\{E_0^1\} + P\{E_{\mathrm{old}}^{\mathrm{Col}}\} & P\{E_{\mathrm{new}}^{\mathrm{Col}}\} \\ P\{E_1^1\}x^2 + P\{E_2^2\}x^2 + P\{E_1^2\}x^2 & 0 & P\{E_0^0\} + P\{E_0^1\} + P\{E_0^2\} \end{pmatrix} \quad (11)$$

TABLE III
EVENTS OCCURRING IN CURRENT SLOT (TWO-DEVICE SA) [39]

event	interpretation
E_m^n	n-collision with m-recovery, $(m \leq n, n = 0,1,2)$
$E_{\mathrm{nop}}^{\mathrm{rec}}$	a packet is recovered, whose replica in the buffer is not *PD*
$E_{\mathrm{pot}}^{\mathrm{rec}}$	only a packet is recovered, whose replica in the buffer is *PD*
E_j^{Col}	j *PD* packets in 2-collision $(j = 0,1,2)$
$E_{\mathrm{new}}^{\mathrm{Col}}$	two-collision occurs with a new *PD* packet
$E_{\mathrm{old}}^{\mathrm{Col}}$	two-collision occurs without a new *PD* packet

V. EVENT PROBABILITIES USING MG DISTRIBUTIONS

In this section, we provide explicit expressions for the event probabilities in Table III for the two-device SA with multi-antenna reception, using the MG distribution, where b_i ($i = 1, 2, \ldots, N$) are integers, as commonly noted in the literature.

The received SNRs from devices 1 and 2 at Ant# i ($i \in \mathcal{L}$) are denoted by γ_{1i} and γ_{2i}, respectively. The RVs γ_{1i}, γ_{2i}, γ_{1j}, and γ_{2j} ($i, j \in \mathcal{L}, i \neq j$) are independent. We derive the event probabilities in Table III for the L-antenna case, which are expressed with the probabilities presented in Section III.

The integral regions for the single-antenna case, shown in Fig. 1, are reused here to facilitate the calculation. For example, region A_i refers to region A at Ant# i, and the associated probability is denoted by P_{A_i}. Owing to symmetry, we have $P_{\Gamma_i} = P_{\check{\Gamma}_i} \triangleq P_{\Gamma}$ with $\Gamma \in \{\mathsf{A}, \mathsf{B}, \mathsf{C}, \mathsf{D}, \mathsf{E}\}$.

In our derivations, we use the following fundamental facts:
(i) RVs γ_{ji} are i.i.d.
(ii) The inclusion-exclusion principle for computing the probability of the union of L sets $A_1, \ldots, A_L$ [52]:

$$\Pr\left(\bigcup_{\ell=1}^{L} A_\ell\right) = \sum_{\emptyset \neq \mathcal{S} \subseteq \{1,\ldots,L\}} (-1)^{|\mathcal{S}|+1} \Pr\left(\bigcap_{\ell \in \mathcal{S}} A_\ell\right). \quad (15)$$

(iii) The binomial theorem: $\sum_{k=0}^{n} \binom{n}{k} x^{n-k} y^k = (x+y)^n$.

A. Closed-Form Expression of $P\{E_m^n\}$

1) $P\{E_2^2\}$: It represents the probability that both packets are successfully decoded in a two-collision. Since the probability that both devices are active in the same slot is p^2, the probability of the event E_2^2 can be described as

$$P\{E_2^2\} = p^2(\Pr\{\Delta\} + \Pr\{\Xi\})$$

$$= p^2 \Big\{ 1 + 2(1 - 2P_{\mathsf{A}} - 2P_{\mathsf{B}} - 2P_{\mathsf{C}} - P_{\mathsf{D}})^L$$

$$- 2(1 - 2P_{\mathsf{A}} - P_{\mathsf{B}} - 2P_{\mathsf{C}} - P_{\mathsf{D}})^L - (1 - 2P_{\mathsf{A}} - 2P_{\mathsf{B}})^L \Big\}. \quad (16)$$

Here, $\Pr\{\Delta\}$ is the probability that two packets P1 and P2 are successfully decoded at any element in $\mathcal{L}$ and $\Pr\{\Xi\}$ is the probability that P1 and P2 are decoded successfully, though not concurrently at an identical antenna element in $\mathcal{L}$. In the following, we deduce the two probabilities and thus (16).

We first consider the case in which both packets are successfully decoded at a single antenna element, denoted Ant# i, where $i \in \mathcal{L}$. The probability of this event is given by

$$\Pr\{\Delta_i\} = \Pr\{\mathsf{A}_i\} + \Pr\{\check{\mathsf{A}}_i\} = 2P_{\mathsf{A}}.$$

The probability that two packets P1 and P2 are successfully decoded at any one in $\mathcal{L}$ is $\Pr\{\Delta\} = \Pr\{\bigcup_{i\in\mathcal{L}} \Delta_i\}$. With the inclusion-exclusion principle (15), we have

$$\Pr\left\{\bigcup_{i\in\mathcal{L}} \Delta_i\right\} = \sum_{\emptyset \neq \mathcal{S} \subseteq \mathcal{L}} (-1)^{|\mathcal{S}|+1} \Pr\left(\bigcap_{i\in\mathcal{S}} \Delta_i\right)$$

$$= \sum_{\ell=1}^{L} \sum_{\substack{\mathcal{S} \subseteq \mathcal{L} \\ |\mathcal{S}| = \ell}} (-1)^{\ell+1} \Pr\left(\bigcap_{i\in\mathcal{S}} \Delta_i\right).$$

Given a fixed $\ell > 0$, there are $\binom{L}{\ell}$ possible subsets $\mathcal{S} \subseteq \mathcal{L}$ such that $|\mathcal{S}| = \ell$. Since the SNRs at the antennas are assumed to be i.i.d., we observe that

$$\Pr\{\Delta\} = \sum_{\ell=1}^{L} (-1)^{\ell+1} \binom{L}{\ell} (\Pr\{\Delta_i\})^\ell = \sum_{\ell=1}^{L} (-1)^{\ell+1} \binom{L}{\ell} (2P_{\mathsf{A}})^\ell.$$

Using the binomial theorem, we rewrite the expression as

$$\Pr\{\Delta\} = -\left(\sum_{\ell=0}^{L} (-1)^\ell \binom{L}{\ell} (2P_{\mathsf{A}})^\ell - 1\right) = 1 - (1 - 2P_{\mathsf{A}})^L.$$

Next, we derive the probability, $\Pr\{\Xi\}$, that P1 and P2 are decoded successfully, though not concurrently at an identical antenna element in $\mathcal{L}$. To this end, we define a simple event $\Xi_{ijp}^{\mathrm{P1}\to\mathrm{P2}}$, where P1 is independently decodable only at Ant# i, P2 is decodable or in a PD state at Ant# j, while neither P1 nor P2 is decodable at Ant# p. This implies that 1) P1 and P2 are decoded independently and successfully at Ant# i, and j, respectively, and 2) the initial decoding of P1 at Ant# i and its subsequent removal at Ant# j enable the exclusive decoding of P2. The event can be represented as follows, for $i \neq j \neq p$,

$$\Xi_{ijp}^{\mathrm{P1}\to\mathrm{P2}} = \mathsf{B}_i \cap \{\check{\mathsf{B}}_j \cup \mathsf{C}_j \cup \check{\mathsf{C}}_j \cup \check{\mathsf{D}}_j\} \cap \overline{\{\mathsf{A}_p \cup \check{\mathsf{A}}_p\}}. \quad (17)$$

Define $\mathcal{L}_1 \subset \mathcal{L}$ as the subset of antenna elements where only P1 is independently decodable within each antenna element. Define $\mathcal{L}_2 \subseteq \mathcal{L} \setminus \mathcal{L}_1$ as the subset where P2 is decodable or in PD state within each antenna element. Further, let $\mathcal{L}_3 = \mathcal{L} \setminus (\mathcal{L}_1 \cup \mathcal{L}_2)$ as the subset, which comprises the remaining antenna elements that cannot decode either P1 or P2. Let $\ell_n = |\mathcal{L}_n|$, $n = 1, 2, 3$. Note that $\mathcal{L}_1 \cup \mathcal{L}_2 \cup \mathcal{L}_3 = \mathcal{L}$ and $\mathcal{L}_{n_1} \cap \mathcal{L}_{n_2} = \emptyset$. $n_1 \neq n_2$.

For any $i \in \mathcal{L}_1, j \in \mathcal{L}_2, p \in \mathcal{L}_3$, the intersection of sets (17) can be written as

$$\bigcap_{\substack{i\in\mathcal{L}_1, j\in\mathcal{L}_2, \\ p\in\mathcal{L}\setminus(\mathcal{L}_1\cup\mathcal{L}_2)}} \Xi_{ijp}^{\mathrm{P1}\to\mathrm{P2}} = \bigcap_{i\in\mathcal{L}_1} \mathsf{B}_i \bigcap_{j\in\mathcal{L}_2} \{\check{\mathsf{B}}_j \cup \mathsf{C}_j \cup \check{\mathsf{C}}_j \cup \check{\mathsf{D}}_j\} \bigcap_{p\in\mathcal{L}\setminus(\mathcal{L}_1\cup\mathcal{L}_2)} \overline{\{\mathsf{A}_p \cup \check{\mathsf{A}}_p\}}$$

$$\triangleq \Xi_{\mathcal{L}_1\mathcal{L}_2}^{\mathrm{P1}\to\mathrm{P2}}.$$

Its probability can be determined by

$$\Pr\{\Xi_{\mathcal{L}_1\mathcal{L}_2}^{P1\to P2}\}$$
$$= \prod_{i\in\mathcal{L}_1}\Pr\{B_i\}\prod_{j\in\mathcal{L}_2}\Pr\{\check{B}_j\cup C_j\cup\check{C}_j\cup\check{D}_j\}\prod_{p\in\mathcal{L}_3}\left(1-\Pr\{A_p\cup\check{A}_p\}\right)$$
$$= P_B^{\ell_1}(P_B+2P_C+P_D)^{\ell_2}(1-2P_A)^{L-\ell_1-\ell_2}.$$

Using the inclusion-exclusion principle (15), we have

$$\Pr\{\Xi^{P1\to P2}\}=\Pr\{\bigcup_{\substack{i,j,p\in\mathcal{L},\\i\neq j\neq p}}\Xi_{ijp}^{P1\to P2}\}$$
$$=\sum_{\substack{\mathcal{L}_1\subset\mathcal{L}\\\mathcal{L}_1\neq\emptyset}}\sum_{\substack{\mathcal{L}_2\subseteq\mathcal{L}\setminus\mathcal{L}_1\\\mathcal{L}_2\neq\emptyset}}(-1)^{|\mathcal{L}_1|+|\mathcal{L}_2|+2}\Pr\{\bigcap_{\substack{i\in\mathcal{L}_1,j\in\mathcal{L}_2,\\p\in\mathcal{L}\setminus(\mathcal{L}_1\cup\mathcal{L}_2)}}\Xi_{ijp}^{P1\to P2}\}$$
$$=\sum_{\ell_1=1}^{L-1}\sum_{\ell_2=1}^{L-\ell_1}(-1)^{\ell_1+\ell_2}\sum_{\substack{\mathcal{L}_1\subset\mathcal{L}\\|\mathcal{L}_1|=\ell_1}}\sum_{\substack{\mathcal{L}_2\subseteq\mathcal{L}\setminus\mathcal{L}_1\\|\mathcal{L}_2|=\ell_2}}\Pr\{\Xi_{\mathcal{L}_1\mathcal{L}_2}^{P1\to P2}\}$$
$$=\sum_{\ell_1=1}^{L-1}\sum_{\ell_2=1}^{L-\ell_1}(-1)^{\ell_1+\ell_2}\binom{L}{\ell_1}\binom{L-\ell_1}{\ell_2}\Pr\{\Xi_{\mathcal{L}_1\mathcal{L}_2}^{P1\to P2}\}.$$

The term $\binom{L}{\ell_1}\binom{L-\ell_1}{\ell_2}$ accounts for the number of distinct antenna pairs $(\mathcal{L}_1,\mathcal{L}_2)$ of sizes ℓ_1 and ℓ_2, respectively, such that $\mathcal{L}_1$ and $\mathcal{L}_2$ are disjoint subsets of $\mathcal{L}$. The symmetrical property of the SNRs for P1 and P2 ensures that $\Pr\{\Xi^{P1\leftarrow P2}\}=\Pr\{\Xi^{P1\to P2}\}$.

Moreover, the probability that P1 and P2 are independently and successfully decoded at each antenna element in their respective $\mathcal{L}_1$ and $\mathcal{L}_2$ is

$$\Pr\{\Xi_{\mathcal{L}_1\mathcal{L}_2}^{P1\to P2}\cap\Xi_{\mathcal{L}_1\mathcal{L}_2}^{P1\leftarrow P2}\}=P_B^{\ell_1+\ell_2}(1-2P_A)^{L-\ell_1-\ell_2}.$$

We thus obtain

$$\Pr\{\Xi\}=\Pr\{\Xi^{P1\to P2}\}+\Pr\{\Xi^{P1\leftarrow P2}\}-\Pr\{\Xi^{P1\to P2}\cap\Xi^{P1\leftarrow P2}\}$$
$$=\sum_{\ell_1=1}^{L-1}\sum_{\ell_2=1}^{L-\ell_1}(-1)^{\ell_1+\ell_2}\binom{L}{\ell_1}\binom{L-\ell_1}{\ell_2}\xi_\Xi(\ell_1,\ell_2)$$

where,

$$\xi_\Xi(\ell_1,\ell_2)=(2P_B^{\ell_1}(P_B+2P_C+P_D)^{\ell_2}-P_B^{\ell_1+\ell_2})$$
$$\cdot(1-2P_A)^{L-\ell_1-\ell_2}.$$

Define $\ell_3=\ell_1+\ell_2$ with $\ell_3\in\{2,3,\ldots,L\}$. It follows that $\binom{L}{\ell_1}\binom{L-\ell_1}{\ell_2}=\binom{L}{\ell_3}\binom{\ell_3}{\ell_1}$. Thus, $\Pr\{\Xi\}$ can be rewritten as

$$\Pr\{\Xi\}=\sum_{\ell_1=1}^{L-1}\sum_{\ell_3=\ell_1+1}^{L}(-1)^{\ell_3}\binom{L}{\ell_3}\binom{\ell_3}{\ell_1}\xi_\Xi(\ell_1,\ell_3-\ell_1)$$
$$=\sum_{\ell_3=2}^{L}\sum_{\ell_1=1}^{\ell_3-1}(-1)^{\ell_3}\binom{L}{\ell_3}\binom{\ell_3}{\ell_1}$$
$$\cdot(2P_B^{\ell_1}(P_B+2P_C+P_D)^{\ell_3-\ell_1}-P_B^{\ell_3})(1-2P_A)^{L-\ell_3}.$$

By applying the binomial theorem to the inner sum over ℓ_1 and the outer sum over ℓ_3, we obtain the following expression.

$$\Pr\{\Xi\}=2(1-2P_A-2P_B-2P_C-P_D)^L-2(1-2P_A-P_B-2P_C-P_D)^L$$
$$-(1-2P_A-2P_B)^L+(1-2P_A)^L.$$

With $\Pr\{\Delta\}$ and $\Pr\{\Xi\}$ we obtain $P\{E_2^2\}$ in (16).

2) $P\{E_1^2\}$: It denotes the probability that either P1 or P2 can be successfully decoded, and can be formulated as

$$P\{E_1^2\}=p^2\left(\Pr\{\Upsilon^{P1}\}+\Pr\{\Upsilon^{P2}\}\right)$$
$$=2p^2\left((P_B+P_D+2P_E)^L-(P_D+2P_E)^L\right).\quad(18)$$

Here, $\Pr\{\Upsilon^{P1}\}$ ($\Pr\{\Upsilon^{P2}\}$) denotes the probability that P1 (P2) is decodable at any one of $\mathcal{L}$, where $\Pr\{\Upsilon^{P1}\}=\Pr\{\Upsilon^{P2}\}$.

We first focus on the case where P1 is decoded. Specifically, we assume that Ant# i ($i\in\mathcal{L}$) exclusively decodes P1, while Ant# $j(\neq i)$ is unable to decode P2, regardless of whether they can decode P1. The event is represented by

$$\Upsilon_{ij}^{P1}=B_i\cap\{B_j\cup D_j\cup E_j\cup\check{E}_j\}.$$

Define $\mathcal{L}_1\subset\mathcal{L}$ as the subset of antenna elements where only P1 can be independently decodable within each antenna element. Define $\mathcal{L}_2\subseteq\mathcal{L}\setminus\mathcal{L}_1$ as the subset comprising the remaining antenna elements that cannot decode P2, regardless of whether they can decode P1. For any $i\in\mathcal{L}_1$, $j\in\mathcal{L}_2$, the intersection of sets Υ_{ij}^{P1} is written as

$$\bigcap_{i\in\mathcal{L}_1,j\in\mathcal{L}\setminus\mathcal{L}_1}\Upsilon_{ij}^{P1}=\bigcap_{i\in\mathcal{L}_1}B_i\bigcap_{j\in\mathcal{L}\setminus\mathcal{L}_1}\{B_j\cup D_j\cup E_j\cup\check{E}_j\}\triangleq\Upsilon_{\mathcal{L}_1}^{P1}.$$

Its probability can be determined by, for $\ell=|\mathcal{L}_1|$,

$$\Pr\{\Upsilon_{\mathcal{L}_1}^{P1}\}=\Pr\left(\bigcap_{i\in\mathcal{L}_1,j\in\mathcal{L}\setminus\mathcal{L}_1}\Upsilon_{ij}^{P1}\right)=(P_B)^\ell(P_B+P_D+2P_E)^{L-\ell}\triangleq\xi_\Upsilon(\ell).$$

The probability of the event $\Pr\{\Upsilon^{P1}\}$ that P1 is successfully decoded at any one in $\mathcal{L}$ is $\Pr\{\Upsilon^{P1}\}=\Pr\{\bigcup_{i,j\in\mathcal{L},i\neq j}\Upsilon_{ij}^{P1}\}$. With (15) and the binomial theorem, we obtain

$$\Pr\{\Upsilon^{P1}\}=\Pr\{\bigcup_{i,j\in\mathcal{L},i\neq j}\Upsilon_{ij}^{P1}\}$$
$$=\sum_{\ell=1}^{L}\sum_{\substack{\mathcal{L}_1\subseteq\mathcal{L}\\|\mathcal{L}_1|=\ell}}(-1)^{\ell+1}\Pr\left(\bigcap_{i\in\mathcal{L}_1,j\in\mathcal{L}\setminus\mathcal{L}_1}\Upsilon_{ij}^{P1}\right)$$
$$=\sum_{\ell=1}^{L}(-1)^{\ell+1}\binom{L}{\ell}\xi_\Upsilon(\ell)$$
$$=(P_B+P_D+2P_E)^L-(P_D+2P_E)^L$$

Using the symmetrical property $\Pr\{\Upsilon^{P1}\}=\Pr\{\Upsilon^{P2}\}$, the probability of the event E_1^2 can be formulated as (18).

3) $P\{E_0^2\}$: Since at Ant# i ($i\in\mathcal{L}$), neither packet can be decoded if the SNR pair $(\gamma_{1i},\gamma_{2i})$ lies in the region $(C_i\cup\check{C}_i\cup D_i\cup\check{D}_i\cup E_i\cup\check{E}_i)$, the probability that neither packet is successfully decoded at any of the antennas in $\mathcal{L}$ is

$$P\{E_0^2\}=p^2\Pr\left(\bigcap_{i\in\mathcal{L}}(C_i\cup\check{C}_i\cup D_i\cup\check{D}_i\cup E_i\cup\check{E}_i)\right)$$
$$=p^2\prod_{i=1}^{L}(P_{C_i}+P_{\check{C}_i}+P_{D_i}+P_{\check{D}_i}+P_{E_i}+P_{\check{E}_i})$$
$$=p^2\{2(P_C+P_D+P_E)\}^L.$$

4) $P\{E_1^1\}, P\{E_1^1\}, P\{E_0^0\}$: When at most one packet is received in the current slot, the probabilities are as follows:

$$P\{E_1^1\} = 2p(1-p)\left(1 - \left(1 - \sum_{n=1}^{N} a_n c_n^{-b_n} \Gamma(b_n, c_n \eta_0)\right)^L\right),$$

$$P\{E_0^1\} = 2p(1-p)\left(\sum_{n=1}^{N} a_n c_n^{-b_n} \gamma(b_n, c_n \eta_0)\right)^L, P\{E_0^0\} = (1-p)^2.$$

B. Closed-Form Expression of $P\{E_j^{\mathrm{Col}}\}$

Let us now focus on the probabilities $P\{E_j^{\mathrm{Col}}\}$ for the existence of j PD packet(s) during a two-collision scenario, where $j = 2, 1, 0$.

1) $P\{E_2^{\mathrm{Col}}\}$: It denotes the probability that both packets P1 and P2 are PD packets, can be formulated as

$$P\{E_2^{\mathrm{Col}}\} = p^2\big(\Pr\{\Theta\} + \Pr\{\Omega\}\big)$$
$$= p^2\big((2P_{\mathsf{C}} + 2P_{\mathsf{D}} + 2P_{\mathsf{E}})^L - 2(P_{\mathsf{D}} + 2P_{\mathsf{E}})^L + (2P_{\mathsf{E}})^L\big). \quad (19)$$

Here, $\Pr\{\Theta\}$ denotes the probability that P1 and P2 are PD packets concurrently at the same antenna element, and $\Pr\{\Omega\}$ is the probability that the packet from one device is a PD packet at one antenna while the packet from the other device is a PD packet at a different antenna.

We subsequently derive (19). In the context of a two-device system, we consider two cases in which 1) both packets are PD packets at the same antenna, and 2) the packet from one device is a PD packet at one antenna, while the packet from the other device is a PD packet at a different antenna.

We first consider the case 1), where both packets are PD packets at a single antenna Ant# $i \in \mathcal{L}$, while at Ant# $j(\neq i)$, neither is successfully decoded. The event is represented by

$$\Theta_{ij} = \big(\mathsf{C}_i \cup \check{\mathsf{C}}_i\big) \cap \big(\mathsf{C}_j \cup \check{\mathsf{C}}_j \cup \mathsf{D}_j \cup \check{\mathsf{D}}_j \cup \mathsf{E}_j \cup \check{\mathsf{E}}_j\big).$$

For simplicity, we reuse notation for analogous subsets in $\mathcal{L}$, with context distinguishing their specific meanings. Let $\mathcal{L}_1 \subset \mathcal{L}$ as the subset of antenna elements where only P1 is in the PD state, and let $\mathcal{L}_2 \subseteq \mathcal{L} \setminus \mathcal{L}_1$ as the subset where P2 is decodable or in PD state within each antenna element. For any $i \in \mathcal{L}_1$, $j \in \mathcal{L}_2$, the intersection of sets Θ_{ij} is written as

$$\bigcap_{i \in \mathcal{L}_1, j \in \mathcal{L} \setminus \mathcal{L}_1} \Theta_{ij} = \bigcap_{i \in \mathcal{L}_1}(\mathsf{C}_i \cup \check{\mathsf{C}}_i) \bigcap_{j \in \mathcal{L} \setminus \mathcal{L}_1}(\mathsf{C}_j \cup \check{\mathsf{C}}_j \cup \mathsf{D}_j \cup \check{\mathsf{D}}_j \cup \mathsf{E}_j \cup \check{\mathsf{E}}_j)$$
$$\triangleq \Theta_{\mathcal{L}_1}.$$

Its probability can be determined by, for $\ell = |\mathcal{L}_1|$,

$$\Pr\{\Theta_{\mathcal{L}_1}\} \triangleq \prod_{i \in \mathcal{L}_1} \Pr\{\mathsf{C}_i \cup \check{\mathsf{C}}_i\} \prod_{j \in \mathcal{L} \setminus \mathcal{L}_1} \Pr\{\mathsf{C}_j \cup \check{\mathsf{C}}_j \cup \mathsf{D}_j \cup \check{\mathsf{D}}_j \cup \mathsf{E}_j \cup \check{\mathsf{E}}_j\}$$
$$= (2P_{\mathsf{C}})^\ell (2P_{\mathsf{C}} + 2P_{\mathsf{D}} + 2P_{\mathsf{E}})^{L-\ell} \triangleq \xi_\Theta(\ell).$$

Using (15) and the binomial theorem, the probability that P1 and P2 are PD packets simultaneously at the same antenna element can be expressed as

$$\Pr\{\Theta\} = \Pr\Big\{\bigcup_{i \in \mathcal{L}_1, j \in \mathcal{L} \setminus \mathcal{L}_1} \Theta_{ij}\Big\} = \sum_{\ell=1}^{L}(-1)^{\ell+1}\binom{L}{\ell}\xi_\Theta(\ell)$$
$$= (2P_{\mathsf{C}} + 2P_{\mathsf{D}} + 2P_{\mathsf{E}})^L - (2P_{\mathsf{D}} + 2P_{\mathsf{E}})^L.$$

We next consider the probability that P1 and P2 are in the PD state at different antenna elements in $\mathcal{L}$. We consider a simple event: P1 is in the PD state at Ant# i and P2 is in the PD state at Ant# j, while at the remaining $L - 2$ antennas neither packet is decoded and they are never in the PD state at the same antenna. The event is expressed as

$$\Omega_{ijp} = \mathsf{D}_i \cap \check{\mathsf{D}}_j \cap \big(\mathsf{D}_p \cup \check{\mathsf{D}}_p \cup \mathsf{E}_p \cup \check{\mathsf{E}}_p\big).$$

We define $\mathcal{L}_1 \subset \mathcal{L}$ ($|\mathcal{L}_1| = \ell_1$) as the subset of antennas where only P1 is in the PD state, and $\mathcal{L}_2 \subseteq \mathcal{L} \setminus \mathcal{L}_1$ ($|\mathcal{L}_2| = \ell_2$) as the subset where only P2 is in the PD state. The remaining antennas form $\mathcal{L}_3 = \mathcal{L} \setminus (\mathcal{L}_1 \cup \mathcal{L}_2)$, where neither P1 nor P2 is decodable and neither is in the PD state.

For any $i \in \mathcal{L}_1, j \in \mathcal{L}_2, p \in \mathcal{L}_3$, the intersection of the sets Ω_{ijp} can be expressed as

$$\bigcap_{\substack{i \in \mathcal{L}_1, j \in \mathcal{L}_2, \\ p \in \mathcal{L} \setminus (\mathcal{L}_1 \cup \mathcal{L}_2)}} \Omega_{ijp} = \bigcap_{i \in \mathcal{L}_1}\mathsf{D}_i \bigcap_{j \in \mathcal{L}_2}\check{\mathsf{D}}_j \bigcap_{p \in \mathcal{L} \setminus (\mathcal{L}_1 \cup \mathcal{L}_2)}\big(\mathsf{D}_p \cup \check{\mathsf{D}}_p \cup \mathsf{E}_p \cup \check{\mathsf{E}}_p\big) \triangleq \Omega(\ell_1, \ell_2).$$

Its probability can be determined by

$$\Pr\{\Omega(\ell_1, \ell_2)\} = \prod_{i \in \mathcal{L}_1}\Pr\{\mathsf{D}_i\} \prod_{j \in \mathcal{L}_2}\Pr\{\check{\mathsf{D}}_j\} \prod_{p \in \mathcal{L}_3}\Pr\{\mathsf{D}_p \cup \check{\mathsf{D}}_p \cup \mathsf{E}_p \cup \check{\mathsf{E}}_p\}$$
$$= (P_{\mathsf{D}})^{\ell_1 + \ell_2}(2P_{\mathsf{D}} + 2P_{\mathsf{E}})^{L-\ell_1-\ell_2} \triangleq \xi_\Omega(\ell_1, \ell_2).$$

With (15), we have

$$\Pr\{\Omega\} = \Pr\Big\{\bigcup_{\substack{i \in \mathcal{L}_1, j \in \mathcal{L}_2 \\ p \in \mathcal{L} \setminus (\mathcal{L}_1 \cup \mathcal{L}_2)}} \Omega_{ijp}\Big\}$$
$$= \sum_{\ell_1=1}^{L-1}\sum_{\ell_2=1}^{L-\ell_1}(-1)^{\ell_1+\ell_2}\binom{L}{\ell_1}\binom{L-\ell_1}{\ell_2}\Pr\Big\{\bigcap_{\substack{i \in \mathcal{L}_1, j \in \mathcal{L}_2 \\ p \in \mathcal{L} \setminus (\mathcal{L}_1 \cup \mathcal{L}_2)}} \Omega_{ijp}\Big\}$$
$$= \sum_{\ell_1=1}^{L-1}\sum_{\ell_2=1}^{L-\ell_1}(-1)^{\ell_1+\ell_2}\binom{L}{\ell_1}\binom{L-\ell_1}{\ell_2}\xi_\Omega(\ell_1, \ell_2)$$
$$= (2P_{\mathsf{E}})^L + \{2(P_{\mathsf{D}} + P_{\mathsf{E}})\}^L - 2(P_{\mathsf{D}} + 2P_{\mathsf{E}})^L.$$

Thus, we obtain (19).

2) $P\{E_1^{\mathrm{Col}}\}$: The probability that one of P1 or P2 is in the PD state, and the other is neither decoded nor in the PD state, can be formulated as

$$P\{E_1^{\mathrm{Col}}\} = p^2\big(\Pr\{\Phi^{\mathrm{P1}}\} + \Pr\{\Phi^{\mathrm{P2}}\}\big)$$
$$= 2p^2\big((P_{\mathsf{D}} + 2P_{\mathsf{E}})^L - (2P_{\mathsf{E}})^L\big). \quad (20)$$

Here, $\Pr\{\Phi^{\mathrm{P1}}\}$ ($\Pr\{\Phi^{\mathrm{P2}}\}$) denotes the probability that only P1 (P2) is in the PD state while P2 (P1) remains undecodable at any one of the antennas in $\mathcal{L}$, where $\Pr\{\Phi^{\mathrm{P1}}\} = \Pr\{\Phi^{\mathrm{P2}}\}$.

We first focus on the case where P1 is in the PD state. Specifically, we assume that P1 is in the PD state at Ant# i ($i \in \mathcal{L}_1$), while P2 is neither in the PD state nor decodable at Ant# j ($j \in \mathcal{L} \setminus \mathcal{L}_1$). The event is expressed as

$$\Phi_{ij}^{\mathrm{P1}} = \mathsf{D}_i \cap \big(\mathsf{D}_j \cup \mathsf{E}_j \cup \check{\mathsf{E}}_j\big).$$

Its probability can be determined by, for $\ell = |\mathcal{L}|$,

$$\Pr\{\Phi_{ij}^{\mathrm{P1}}\} = \Pr\Big(\bigcap_{i \in \mathcal{L}_1, j \in \mathcal{L} \setminus \mathcal{L}_1} \Phi_{ij}^{\mathrm{P1}}\Big) = (P_{\mathsf{D}})^\ell (P_{\mathsf{D}} + 2P_{\mathsf{E}})^{L-\ell} \triangleq \xi_\Phi(\ell).$$

The probability of the event $\Pr\{\Phi^{\text{P1}}\}$, where only P1 is in the PD state and P2 is undecodable at any one of the antennas in $\mathcal{L}$ is $\Pr\{\Phi^{\text{P1}}\} = \Pr\{\bigcup_{i,j\in\mathcal{L},j\neq i}\Phi^{\text{P1}}_{ij}\}$. With (15) and the binomial theorem, we obtain

$$
\begin{aligned}
\Pr\{\Phi^{\text{P1}}\} &= \Pr\Big\{\bigcup_{\substack{i,j\in\mathcal{L}\\ j\neq i}}\Phi^{\text{P1}}_{ij}\Big\}\\
&= \sum_{\ell=1}^{L}(-1)^{\ell+1}\binom{L}{\ell}\xi_\Phi(\ell)\\
&= (P_{\text{D}}+2P_{\text{E}})^L - (2P_{\text{E}})^L.
\end{aligned}
$$

Using the symmetrical property $\Pr\{\Phi^{\text{P1}}\} = \Pr\{\Phi^{\text{P2}}\}$, the probability of the event E^{Col}_1 is obtained in (20).

3) $P\{E^{\text{Col}}_0\}$: The event E^{Col}_0 refers to the case where both packets P1 and P2 are neither decodable nor in the PD state. Since P1 and P2 satisfy the condition at Ant# i only when the SNR pair $(\gamma_{1i},\gamma_{2i})$ lies in the region $(\mathsf{E}_i\cup\check{\mathsf{E}}_i)$, the probability that neither packet is decodable nor in the PD state at any of the antennas in $\mathcal{L}$ is calculated as

$$
P\{E^{\text{Col}}_0\} = p^2\Pr\Big(\bigcap_{i\in\mathcal{L}}(\mathsf{E}_i\cup\check{\mathsf{E}}_i)\Big) = p^2\prod_{i=1}^{L}(P_{\mathsf{E}_i}+P_{\check{\mathsf{E}}_i}) = p^2(2P_{\mathsf{E}})^L.
$$

C. $P\{E^{\text{rec}}_{\text{pot}}\}$, $P\{E^{\text{rec}}_{\text{nop}}\}$, $P\{E^{\text{Col}}_{\text{new}}\}$, and $P\{E^{\text{Col}}_{\text{old}}\}$

The remaining probabilities in Table III are given as follows [39], with their derivations omitted due to space constraints.

$$
\begin{aligned}
P\{E^{\text{rec}}_{\text{pot}}\} &= (P\{E^1_1\}+P\{E^2_1\})/2\\
P\{E^{\text{rec}}_{\text{nop}}\} &= (P\{E^1_1\}+P\{E^2_1\})/2 + P\{E^2_2\}\\
P\{E^{\text{Col}}_{\text{new}}\} &= P\{E^{\text{Col}}_1\}/2 + P\{E^{\text{Col}}_2\}\\
P\{E^{\text{Col}}_{\text{old}}\} &= P\{E^{\text{Col}}_1\}/2 + P\{E^{\text{Col}}_0\}.
\end{aligned}
$$

D. Optimization of Probability p and code rate R

Before concluding this section, we aim to optimize transmission probability p and channel code rate R. This optimization ensures that the sum rate of (14) is maximized for the given average received SNR $\bar{\gamma}$ and the number of antennas L.

$$
\begin{aligned}
&\underset{0 < p \leq 1, R > 0}{\text{maximize}} && R_s = R\cdot T(p,R,\bar{\gamma},L).\\
&\text{subject to} && \bar{\gamma},\ L \text{ are constant.}
\end{aligned}
\tag{21}
$$

In previous studies, R has typically been restricted to $R \geq 1$ due to complexity [39], [50]. A notable contribution of this work is that, by clarifying the integration range in Section III-C, we obtain the exact optimization expression (21) for the broader condition $R > 0$.

E. Asymptotic Sum Rate

We derive an asymptotic ($L\to\infty$) sum rate, given by

$$
R^{(\infty)}_s = \lim_{L\to\infty}R_s = \lim_{L\to\infty}R\cdot T(p,R,\bar{\gamma},L) = 2pR. \tag{22}
$$

The derivation of $R^{(\infty)}_s$ can be found in Appendix II. Since $R^{(\infty)}_s$ increases monotonically with respect to p, the transmission probability of $p = 1$ is always the optimal setting.

TABLE IV
SPECIFICATIONS IN ANALYSIS AND SIMULATIONS

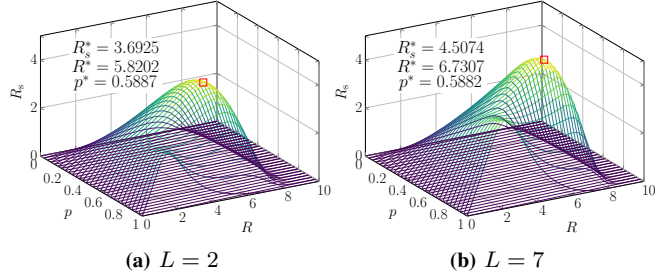| Rician factor	$K = 3$	# of MG terms	$N = 20$
average received SNR per device	$\bar{\gamma} = 20$ dB	# of slots	$n_s = 10^4$
# of simulation experiments	10^3	# of devices	$K_{\text{T}} = 2$

(a) $L = 2$ **(b)** $L = 7$

Fig. 6. For $L = 2$ and $L = 7$ antennas, the sum rate R_s is evaluated with different values of p and R under 20 dB. Markers $\square$ indicate the optimized results in (21).

Remark 2. *The collision channel model [38] focuses solely on packet collisions. Multi packet reception (MPR) channels [22], [53], [54] extend this model. In a simple two-MPR channel, it is assumed that an AP can successfully decode two packets in the slots. In a two-device SA with a single-antenna AP, the sum rate over a two-MPR channel is $2pR$, aligning with our asymptotic result in (22).*

VI. NUMERICAL AND SIMULATION RESULTS

In this section, we present numerical results for the sum rate and its maximum obtained by optimizing the transmission probability and code rate, and we validate the derived expressions through simulations.

A. Two-Device SA

As stated in Section II, the PDFs of some distributions, such as the Hoyt and Rician distributions, contain special functions, and thus performance analysis is complicated or intractable. The MG model offers an approximate solution for these distributions [42]. In this work, as an example of the MG model, we consider the Rician fading channel and provide an approximate sum rate (Section IV). Throughout this section, without specific declarations, the default parameters adopted to derive the results are reported in Table IV.

Figure 6 illustrates the sum rate in (14) as a function of R and p for $L = 2$ and $L = 7$. The optimal parameters R^* and p^* that maximize the sum rate R_s in (21) are determined using the Sequential Quadratic Programming (SQP) algorithm [55]. As shown in Fig. 6(a), when $\bar{\gamma} = 20$ dB and $L = 2$, the maximum sum rate $R^*_s = 3.6925$ is achieved at $(p^* = 0.5887,\ R^* = 5.8202)$. In addition, when the number of antennas is increased to $L = 7$, R^*_s improves to 4.5074 (see Fig. 6(b)).

Table V summarizes the maximum sum rate achieved in the two-device SA with real-time feedback on different fading models, including the Rayleigh [39], Nakagami-m [50], and Rician channels, with varying numbers of antennas. Each fading model is evaluated based on its corresponding SNR distribution with the MG parameters presented in Table I.
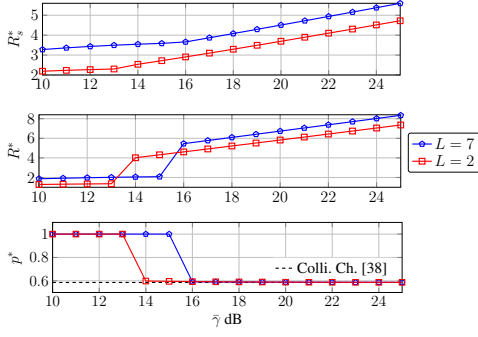
Fig. 7. The maximum sum rate R_s^* and optimized parameters (p^*, R^*) vs. received SNR $\bar{\gamma}$ ($L = 2$ and 7).
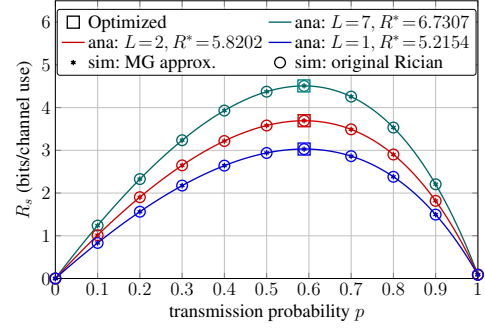

Fig. 8. The sum rate for $L = 1$, 2 and 7 under $K = 3$ and $\bar{\gamma} = 20$ dB. Analysis and simulation with MG, as well as simulation with the original Rician distribution.
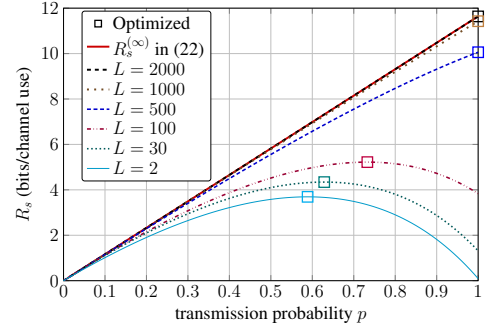

Fig. 9. The sum rate for various values of L under $K = 3$, $\bar{\gamma} = 20$ dB, and a fixed code rate $R = 5.8202$. Also, the asymptotic sum rate is shown.

Note that the SNR distribution corresponding to the Rician model is approximated by the MG distribution approach. For Nakagami-m and Rician fading channels in our numerical examples, the fading parameters are $m = 2$ and $K = 3$, respectively. As shown in Table V, when $L = 1$, Rayleigh fading channels exhibit inferior performance compared to Nakagami-m and Rician fading channels, owing to different power ratios between dominant and scattered components. In contrast, when the number of antennas is increased to $L = 2$, Rayleigh shows a performance gain of 31.50%, while Nakagami-m and Rician improve by 20.96% and 21.86%, respectively. This result indicates that Rayleigh fading, due to its higher degree of randomness, achieves greater spatial diversity gains than those of Nakagami-m and Rician fading channels. Furthermore, when $L \geq 5$, Rayleigh fading outperforms both Nakagami-m and Rician fading channels.

Another important aspect to be examined is how the maximum sum rate R_s^* and the optimized parameters (p^*, R^*) are affected by the received SNR $\bar{\gamma}$. Figure 7 depicts R_s^*, R^*, and p^* for different $\bar{\gamma}$. R_s^* increases monotonically with $\bar{\gamma}$. A fundamental trade-off arises between R^* and p^*. In the low-SNR regime, a low code rate is chosen to mitigate channel fading, and consequently, a high transmission probability ($p = 1$) becomes optimal. In contrast, in the high-SNR regime, the effect of channel fading is largely mitigated, enabling a higher code rate. However, the increased code rate raises the decoding threshold, making collisions more difficult to resolve; thus, collisions become the dominant limiting factor and reduce the optimal transmission probability. As the SNR becomes sufficiently large, the optimal transmission probability converges to the value of $p^* = 0.5858$ in the collision channel [38], while R^* increases monotonically. Moreover, owing to the diversity gain, increasing the number of antennas allows a high transmission probability to be sustained at higher SNRs compared with the case of fewer antennas.

In the Rician fading channel model, Fig. 8 shows the numerical results of the maximum sum rate for $L = 1$, 2, and 7 under their corresponding optimal code rates and $\bar{\gamma} = 20$ dB. Moreover, we conducted two types of simulations ($n_s = 10^4$) to compute the sum rates: 1) The random numbers are generated from the MG distribution, denoted by $*$ in the figure. Specifically, among the N random numbers sampled from their corresponding Gamma distributions, respectively,

select one with weighted probabilities; 2) SNR values are sampled from the original Rician distribution [44], denoted by $\circ$. Two simulations and the numerical results show an excellent match. For $L = 1$, the maximum sum rate is $R_s^* = 2.8672$. When $L = 2$ and $L = 7$, R_s^* increases to 3.6925 and 4.0732, respectively, confirming the performance gain from multiple antennas.

In Fig. 9, we examine the asymptotic sum rate $R_s^{(\infty)}$ derived in (22). We fix the code rate R to 5.8202 and evaluate the sum rate (14). It improves with the increase of L, approaching the asymptotic value of $2R = 11.6404$ when $L = 2000$. The p^* increases with L, as a larger number of antennas enhances the probability of successful decoding due to spatial diversity.

Figure 10 examines the case of $R < 1$ and evaluates the sum rate with $R = 0.95$ as an example under $\bar{\gamma} = -2$ dB. As discussed in Section III, the probability derivations are integrated into the general condition $R > 0$, which simplifies the sum-rate analysis. Notably, for $0 < R < 1$, the numerical results remain consistent with the simulations.

In Fig. 11, we present the results of two-device SA with only the intra-slot SIC. Without the inter-slot SIC, the throughput is represented as $T = \mathrm{d}p_{S_0,S_0}(x)/\mathrm{d}x|_{x=1} = P\{E_1^1\} + P\{E_1^2\} + 2P\{E_2^2\}$, which is the entry $(P'(1))_{(0,0)}$ in (12). It can be observed that inter-slot SIC improves the sum rate. The improvement is more significant with $L = 2$.

B. Multi-Device SA

We have so far presented numerical results based on the theoretical analysis of the two-device case. For $K_T(> 2)$

TABLE V
THE MAXIMUM SUM RATE R_s^* WITH OPTIMAL PARAMETERS (p^*, R^*) AT DIFFERENT VALUES OF L OVER DIFFERENT FADING MODELS ($\bar{\gamma} = 20$ dB).

	Rayleigh			Nakagami-m ($m = 2$)			Rician ($K = 3$)		
L	p^*	R^*	R_s^*	p^*	R^*	R_s^*	p^*	R^*	R_s^*
1	0.6087	4.7309	2.6131 [39]	0.5868	5.1129	3.0015 [50]	0.5887	5.2154	3.0302
2	0.6105	5.3756	3.4360	0.5865	5.7542	3.6307	0.5887	5.8202	3.6925
5	1.0000	2.7982	4.4434	0.5862	6.4854	4.2700	0.5883	6.5172	4.3290

Fig. 10. The sum rate for $L = 1$, 2, and 3 under $K = 3$, $R = 0.95$, and $\bar{\gamma} = -2$ dB.

Fig. 12. R_s^* for different K_{T} and L under $\bar{\gamma} = 20$ dB. The simulation results are averaged over 10^2 independent experiments, each consisting of $n_s = 10^3$ slots.
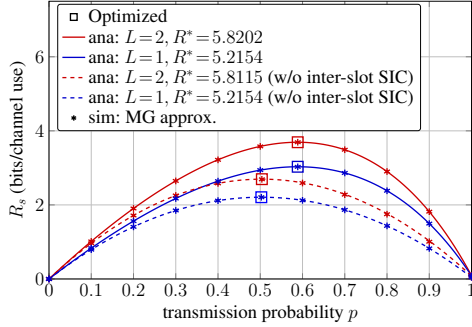

Fig. 11. The sum rate under optimized code rate R^* and $\bar{\gamma} = 20$ dB, with and without inter-slot SIC for $L = 1$ and 2.

devices, however, only simulation results can be obtained, since the state space of the Markov process grows rapidly with K_{T}. We search for (p^*, R^*) that maximize R_s^*. Here, R_s^* denotes the average sum rate over n_s slots. Figure 12 indicates that the spatial diversity provided by multiple antennas is also a key to efficiently accommodating larger device populations.

VII. CONCLUSION

We have presented a comprehensive analytical framework for evaluating the performance of spatio-temporal SIC-based slotted ALOHA systems with multi-antenna reception over mixture Gamma fading channels. By applying the inclusion–exclusion principle to the multi-antenna reception scenario, we derived closed-form state-transition probabilities for the two-device case. These expressions enable exact computation of the average sum rate through a Markov-based formulation and facilitate the joint optimization of the transmission probability and code rate. The analytical results show excellent agreement with simulations, validating the proposed model and quantitatively demonstrating the performance gains achieved by multi-antenna reception. Although we have illustrated the analysis using the Rician fading case, the proposed
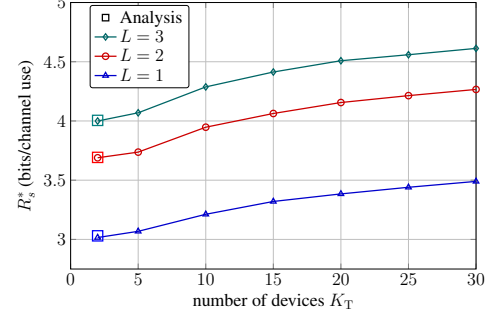
framework is readily extendable to other fading distributions. Deriving analytical results for multi-device scenarios remains a challenging problem, even under single-antenna reception. Furthermore, analyzing IRSA with multi-antenna reception constitutes an interesting direction for future research.

APPENDIX I
CLOSED-FORM PROBABILITY EXPRESSIONS

A. $R \geq 1$

We present analytical probability expressions for the regions shown in Fig. 1. Due to symmetry, we focus on the range where $\gamma_1 > \gamma_2$.

We formulate the probability P_{A} as

$$P_{\mathsf{A}} = \Pr\{\mathsf{A} : (\gamma_1, \gamma_2) | \gamma_1 > \eta_0(1 + \gamma_2), \gamma_2 > \eta_0\}$$
$$= \int_{\eta_0}^{\infty} p(\gamma_2) \int_{\eta_0(1+\gamma_2)}^{\infty} p(\gamma_1) \mathrm{d}\gamma_1 \mathrm{d}\gamma_2. \qquad (23)$$

The integral concerning γ_1 is

$$\int_{\eta_0(1+\gamma_2)}^{\infty} p(\gamma_1) \mathrm{d}\gamma_1 = \sum_{n=1}^{N} a_n c_n^{-b_n} \Gamma(b_n, c_n(\eta_0(1 + \gamma_2)))$$
$$= \sum_{n=1}^{N} a_n c_n^{-b_n} (b_n - 1)! e^{-c_n \eta_0 (1+\gamma_2)} \sum_{k_1=0}^{b_n-1} \frac{(c_n \eta_0)^{k_1} (1 + \gamma_2)^{k_1}}{k_1!}$$
$$\stackrel{(a)}{=} \sum_{n=1}^{N} d_n e^{-c_n \eta_0} e^{-c_n \eta_0 \gamma_2} \sum_{k_1=0}^{b_n-1} \left(\frac{(c_n \eta_0)^{k_1}}{k_1!} \sum_{k_2=0}^{k_1} \binom{k_1}{k_2} \gamma_2^{k_2} \right).$$

In (a), we use the binomial expansion $(1+x)^n = \sum_{k=0}^{n} \binom{n}{k} x^k$. In (23), we then integrate with respect to γ_2

$$\int_{\eta_0}^{\infty} p(\gamma_2) e^{-c_n \eta_0 (\gamma_2)} \gamma_2^{k_2} \mathrm{d}\gamma_2$$
$$= \sum_{m=1}^{N} a_m \int_{\eta_0}^{\infty} \gamma_2^{b_m+k_2-1} e^{-(c_n \eta_0 + c_m)\gamma_2} \mathrm{d}\gamma_2$$

$$= \sum_{m=1}^{N} a_m (c_n \eta_0 + c_m)^{-(b_m+k_2)} \Gamma(b_m + k_2, (c_n \eta_0 + c_m)\eta_0).$$

Thus, the probability that both devices are successful in the slot is:

$$P_{\mathsf{A}} = \sum_{n=1}^{N} d_n e^{-c_n \eta_0} \sum_{k_1=0}^{b_n-1} \left(\frac{(c_n \eta_0)^{k_1}}{k_1!} \sum_{k_2=0}^{k_1} \binom{k_1}{k_2} \right. \tag{24}$$

$$\left. \cdot \sum_{m=1}^{N} a_m (c_n \eta_0 + c_m)^{-(b_m+k_2)} \Gamma(b_m + k_2, (c_n \eta_0 + c_m)\eta_0) \right).$$

Similarly, we derive P_{B} through P_{E} as follows.

$$P_{\mathsf{B}} = \sum_{n=1}^{N} d_n e^{-c_n \eta_0} \sum_{k_1=0}^{b_n-1} \left(\frac{(c_n \eta_0)^{k_1}}{k_1!} \sum_{k_2=0}^{k_1} \binom{k_1}{k_2} \right.$$

$$\left. \cdot \sum_{m=1}^{N} a_m (c_n \eta_0 + c_m)^{-(b_m+k_2)} \gamma(b_m + k_2, (c_n \eta_0 + c_m)\eta_0) \right),$$

$$P_{\mathsf{C}} = \sum_{n=1}^{N} d_n \sum_{k_1=0}^{b_n-1} \frac{c_n^{k_1}}{k_1!} \sum_{m=1}^{N} a_m (c_n + c_m)^{-(b_m+k_1)} \Gamma(b_m + k_1, (c_n + c_m)\eta_0)$$

$$- \sum_{n=1}^{N} d_n e^{-c_n \eta_0} \sum_{k_1=0}^{b_n-1} \left(\frac{(c_n \eta_0)^{k_1}}{k_1!} \sum_{k_2=0}^{k_1} \binom{k_1}{k_2} \right. \tag{25}$$

$$\left. \cdot \sum_{m=1}^{N} a_m (c_n \eta_0 + c_m)^{-(b_m+k_2)} \Gamma(b_m + k_2, (c_n \eta_0 + c_m)\eta_0) \right),$$

$$P_{\mathsf{D}} = \sum_{n=1}^{N} d_n e^{-c_n \eta_0} \left(\sum_{k_1=0}^{b_n-1} \frac{(c_n \eta_0)^{k_1}}{k_1!} \right) \left(\sum_{m=1}^{N} a_m c_m^{-b_m} \gamma(b_m, c_m \eta_0) \right)$$

$$- \sum_{n=1}^{N} d_n e^{-c_n \eta_0} \sum_{k_1=0}^{b_n-1} \left(\frac{(c_n \eta_0)^{k_1}}{k_1!} \sum_{k_2=0}^{k_1} \binom{k_1}{k_2} \right.$$

$$\left. \cdot \sum_{m=1}^{N} a_m (c_n \eta_0 + c_m)^{-(b_m+k_2)} \gamma(b_m + k_2, (c_n \eta_0 + c_m)\eta_0) \right),$$

$$P_{\mathsf{E}} = \sum_{n=1}^{N} d_n \sum_{k_1=0}^{b_n-1} \frac{c_n^{k_1}}{k_1!} \sum_{m=1}^{N} a_m (c_n + c_m)^{-(b_m+k_1)} \gamma(b_m + k_1, (c_n + c_m)\eta_0)$$

$$- \sum_{n=1}^{N} d_n e^{-c_n \eta_0} \left(\sum_{k_1=0}^{b_n-1} \frac{(c_n \eta_0)^{k_1}}{k_1!} \right) \left(\sum_{m=1}^{N} a_m c_m^{-b_m} \gamma(b_m, c_m \eta_0) \right).$$

B. $0 < R < 1$

We present analytical expressions of $P_{(\mathsf{A'} \cup \mathsf{F'})}$ and $P_{\mathsf{C'}}$, whose corresponding regions are shown in Fig. 2.

For region $\mathsf{\breve{F}'}$, We have the probability:

$$P_{\mathsf{\breve{F}'}} = \Pr \left\{ \mathsf{\breve{F}'} : (\gamma_1, \gamma_2) | \eta_0(1 + \gamma_2) < \gamma_1 < \gamma_2, \gamma_2 > \frac{\eta_0}{1-\eta_0} \right\}$$

$$= \sum_{n=1}^{N} d_n e^{-c_n \eta_0} \left\{ \sum_{k_1=0}^{b_n-1} \frac{(c_n \eta_0)^{k_1}}{k_1!} \sum_{k_2=0}^{k_1} \binom{k_1}{k_2} \right. \tag{26}$$

$$\cdot \sum_{m=1}^{N} a_m (c_n \eta_0 + c_m)^{-(b_m+k_2)} \Gamma(b_m + k_2, \frac{(c_n \eta_0 + c_m)\eta_0}{1-\eta_0})$$

$$\left. - \sum_{k=0}^{b_n-1} \frac{c_n^k}{k!} \sum_{m=1}^{N} a_m (c_n + c_m)^{-(b_m+k)} \Gamma(b_m + k, \frac{(c_n + c_m)\eta_0}{1-\eta_0}) \right\}.$$

Since $P_{(\mathsf{A'} \cup \mathsf{F'})} = P_{\mathsf{A'} \cup \mathsf{F'} \cup \mathsf{\breve{F}'}} - P_{\mathsf{\breve{F}'}}$ and $P_{\mathsf{A'} \cup \mathsf{F'} \cup \mathsf{\breve{F}'}}$ has the same form as in (26), we have

$$P_{(\mathsf{A'} \cup \mathsf{F'})} = \sum_{n=1}^{N} d_n e^{-c_n \eta_0} \sum_{k_1=0}^{b_n-1} \frac{(c_n \eta_0)^{k_1}}{k_1!} \sum_{k_2=0}^{k_1} \binom{k_1}{k_2} \sum_{m=1}^{N} a_m (c_n \eta_0 + c_m)^{-(b_m+k_2)}$$

$$\cdot \left\{ \Gamma(b_m + k_2, (c_n \eta_0 + c_m)\eta_0) - \Gamma(b_m + k_2, \frac{(c_n \eta_0 + c_m)\eta_0}{1-\eta_0}) \right\}$$

$$+ \sum_{n=1}^{N} d_n e^{-c_n \eta_0} \sum_{k=0}^{b_n-1} \frac{c_n^k}{k!} \sum_{m=1}^{N} a_m (c_n + c_m)^{-(b_m+k)}$$

$$\cdot \Gamma(b_m + k, \frac{(c_n + c_m)\eta_0}{1-\eta_0}). \tag{27}$$

Moreover, the closed-form probability over region $\mathsf{C'}$ is

$$P_{\mathsf{C'}} = \sum_{n=1}^{N} d_n \sum_{k=0}^{b_n-1} \frac{c_n^k}{k!} \sum_{m=1}^{N} a_m (c_m + c_n)^{-(b_m+k)} \tag{28}$$

$$\cdot \left\{ \gamma(b_m + k, \frac{(c_m + c_n)\eta_0}{1-\eta_0}) - \gamma(b_m + k, (c_m + c_n)\eta_0) \right\}$$

$$- \sum_{n=1}^{N} d_n e^{-c_n \eta_0} \sum_{k_1=0}^{b_n-1} \frac{(c_n \eta_0)^{k_1}}{k_1!} \sum_{k_2=0}^{k_1} \binom{k_1}{k_2} \sum_{m=1}^{N} a_m (c_m + c_n \eta_0)^{-(b_m+k_2)}$$

$$\cdot \left\{ \gamma(b_m + k_2, \frac{(c_m + c_n \eta_0)\eta_0}{1-\eta_0}) - \gamma(b_m + k_2, (c_m + c_n \eta_0)\eta_0) \right\}.$$

Finally, as stated at the end of Section III, we merge $P_{(\mathsf{A'} \cup \mathsf{F'})}$ of (27) and P_{A} of (24) to P_{A} in (29) including both cases of $R > 1$ and $0 < R < 1$. Similarly, in (30) we replace $P_{\mathsf{C'}}$ of (28) with P_{C} for $0 < R < 1$.

APPENDIX II
DERIVATION OF (22)

Recalling that $2(P_{\mathsf{A}} + P_{\mathsf{B}} + P_{\mathsf{C}} + P_{\mathsf{D}} + P_{\mathsf{E}}) = 1$, we can easily obtain from (16) that $\lim_{L \to \infty} P\{E_2^2\} = p^2$. Similarly, we have $\lim_{L \to \infty} P\{E_1^1\} = 2p(1-p)$, $\lim_{L \to \infty} P\{E_0^0\} = (1-p)^2$, $\lim_{L \to \infty} P\{E_{\text{pot}}^{\text{rec}}\} = p(1-p)$, $\lim_{L \to \infty} P\{E_{\text{nop}}^{\text{rec}}\} = p^2 + p(1-p)$ and all other probabilities tend to zero as $L \to \infty$. Therefore, the limit of (12) can be written as

$$\lim_{L \to \infty} \mathbf{P'}(1) = \begin{pmatrix} 2p^2 + 2p(1-p) & 0 & 0 \\ 2p^2 + 3p(1-p) & 0 & 0 \\ 2p^2 + 4p(1-p) & 0 & 0 \end{pmatrix}.$$

In addition, $\lim_{L \to \infty} P\{E_1^{\text{Col}}\} = 0$ and $\lim_{L \to \infty} P\{E_2^{\text{Col}}\} = 0$, indicating that in (11) the transitions from state S_0 to S_1 and S_2 become negligible as $L \to \infty$. Consequently, the stationary distribution converges to $(w_0, w_1, w_2)^{\mathrm{T}} = (1, 0, 0)^{\mathrm{T}}$. Hence, the throughput of (13) becomes $T(p, R, \bar{\gamma}, L \to \infty) = 2p$, and thus the asymptotic sum rate in (22) is obtained.

REFERENCES

[1] N. H. Mahmood, H. Alves, O. A. López, M. Shehab, D. P. M. Osorio, and M. Latva-Aho, "Six key features of machine type communication in 6G," in *Proc. 2nd 6G Wireless Summit (6G SUMMIT)*, 2020, pp. 1–5.

[2] Y. Polyanskiy, "A perspective on massive random-access," in *Proc. IEEE Int. Symp. Inf. Theory (ISIT)*, 2017, pp. 2523–2527.

[3] A. Munari, "Modern random access: An age of information perspective on irregular repetition slotted ALOHA," *IEEE Trans. Commun.*, vol. 69, no. 6, pp. 3572–3585, 2021.

[4] N. Abramson, "The ALOHA system: Another alternative for computer communications," in *Proc. AFIPS Fall Joint*, 1970, pp. 281–285.

$$P_{\mathsf{A}} = \begin{cases} \sum_{n=1}^{N} d_n e^{-c_n \eta_0} \sum_{k_1=0}^{b_n-1} \frac{(c_n \eta_0)^{k_1}}{k_1!} \sum_{k_2=0}^{k_1} \binom{k_1}{k_2} \sum_{m=1}^{N} a_m (c_n \eta_0 + c_m)^{-(b_m+k_2)} \left\{ \Gamma(b_m+k_2, (c_n \eta_0 + c_m)\eta_0) - \Gamma(b_m+k_2, \frac{(c_n\eta_0+c_m)\eta_0}{1-\eta_0}) \right\} \\ + \sum_{n=1}^{N} d_n e^{-c_n \eta_0} \sum_{k=0}^{b_n-1} \frac{c_n^k}{k!} \sum_{m=1}^{N} a_m (c_n+c_m)^{-(b_m+k)} \Gamma(b_m+k, \frac{(c_n+c_m)\eta_0}{1-\eta_0}) \\ \sum_{n=1}^{N} d_n e^{-c_n \eta_0} \sum_{k_1=0}^{b_n-1} \left(\frac{(c_n\eta_0)^{k_1}}{k_1!} \sum_{k_2=0}^{k_1} \binom{k_1}{k_2} \sum_{m=1}^{N} a_m (c_n\eta_0+c_m)^{-(b_m+k_2)} \Gamma(b_m+k_2, (c_n\eta_0+c_m)\eta_0) \right), \end{cases}$$

$$\begin{aligned} & 0 < R < 1 \\ & R \ge 1, \end{aligned}$$

(29)

$$P_{\mathsf{C}} = \begin{cases} \sum_{n=1}^{N} d_n \sum_{k=0}^{b_n-1} \frac{c_n^k}{k!} \sum_{m=1}^{N} a_m (c_m+c_n)^{-(b_m+k)} \left\{ \gamma(b_m+k, \frac{(c_m+c_n)\eta_0}{1-\eta_0}) - \gamma(b_m+k, (c_m+c_n)\eta_0) \right\} \\ - \sum_{n=1}^{N} d_n e^{-c_n\eta_0} \sum_{k_1=0}^{b_n-1} \frac{(c_n\eta_0)^{k_1}}{k_1!} \sum_{k_2=0}^{k_1} \binom{k_1}{k_2} (c_m+c_n\eta_0)^{-(b_m+k_2)} \left\{ \gamma(b_m+k_2, \frac{(c_m+c_n\eta_0)\eta_0}{1-\eta_0}) - \gamma(b_m+k_2, (c_m+c_n\eta_0)\eta_0) \right\} \\ \sum_{n=1}^{N} d_n \sum_{k_1=0}^{b_n-1} \frac{c_n^{k_1}}{k_1!} \sum_{m=1}^{N} a_m (c_n+c_m)^{-(b_m+k_1)} \Gamma(b_m+k_1, (c_n+c_m)\eta_0) \\ - \sum_{n=1}^{N} d_n e^{-c_n\eta_0} \sum_{k_1=0}^{b_n-1} \frac{(c_n\eta_0)^{k_1}}{k_1!} \sum_{k_2=0}^{k_1} \binom{k_1}{k_2} \sum_{m=1}^{N} a_m (c_n\eta_0+c_m)^{-(b_m+k_2)} \Gamma(b_m+k_2, (c_n\eta_0+c_m)\eta_0) \right), \end{cases}$$

$$\begin{aligned} & 0 < R < 1, \\ & R \ge 1. \end{aligned}$$

(30)

[5] B. Hajek and T. van Loon, "Decentralized dynamic control of a multiaccess broadcast channel," *IEEE Trans. Autom. Control*, vol. 27, no. 3, pp. 559–569, 1982.

[6] D. P. Bertsekas and R. G. Gallager, *Data Networks*, 2nd ed. Englewood Cliffs, NJ, USA: Prentice Hall, 1992.

[7] L. G. Roberts, "ALOHA packet system with and without slots and capture," *SIGCOMM Comput.*, vol. 5, no. 2, pp. 28–42, 1975.

[8] J. Metzner, "On improving utilization in ALOHA networks," *IEEE Trans. Commun.*, vol. 24, no. 4, pp. 447–448, 1976.

[9] N. Abramson, "The throughput of packet broadcasting channels," *IEEE Trans. Commun.*, vol. 25, no. 1, pp. 117–128, 1977.

[10] G. D. Nguyen, A. Ephremides, and J. E. Wieselthier, "On capture in random-access systems," in *Proc. IEEE Int. Symp. Inf. Theory (ISIT)*, 2006, pp. 2072–2076.

[11] A. Zanella and M. Zorzi, "Theoretical analysis of the capture probability in wireless systems with multiple packet reception capabilities," *IEEE Trans. Commun.*, vol. 60, no. 4, pp. 1058–1071, 2012.

[12] S. A. Tegos, P. D. Diamantoulakis, A. S. Lioumpas, P. G. Sarigiannidis, and G. K. Karagiannidis, "Slotted ALOHA with NOMA for the next generation IoT," *IEEE Trans. Commun.*, vol. 68, no. 10, pp. 6289–6301, 2020.

[13] C. Xu, L. Ping, P. Wang, S. Chan, and X. Lin, "Decentralized power control for random access with successive interference cancellation," *IEEE J. Sel. Areas Commun.*, vol. 31, no. 11, pp. 2387–2396, 2013.

[14] D. Tse and P. Viswanath, *Fundamentals of Wireless Communication*. USA: Cambridge University Press, 2005.

[15] M. Zorzi, "Mobile radio slotted ALOHA with capture and diversity," in *Proc. IEEE INFOCOM*, vol. 1, 1995, pp. 121–128.

[16] M. Zorzi, "Mobile radio slotted ALOHA with capture, diversity and retransmission control in the presence of shadowing," *Wireless Netw.*, vol. 4, pp. 379–388, 1998.

[17] A. Munari, M. Heindlmaier, G. Liva, and M. Berioli, "The throughput of slotted ALOHA with diversity," in *Proc. 51st Annu. Allerton Conf. Commun., Control, Comput. (Allerton)*, 2013, pp. 698–706.

[18] A. Munari, F. Clazzer, G. Liva, and M. Heindlmaier, "Multiple-relay slotted ALOHA: Performance analysis and bounds," *IEEE Trans. Commun.*, vol. 69, no. 3, pp. 1578–1594, 2020.

[19] P. Li, X. Jian, F. Wang, S. Fu, and Z. Zhang, "Theoretical throughput analysis for massive random access with spatial successive decoding," *IEEE Trans. Veh. Technol.*, vol. 69, no. 7, pp. 7998–8002, 2020.

[20] A. Mastilovic, D. Vukobratovic, D. Jakovetic, and D. Bajovic, "Co-operative slotted ALOHA for massive M2M random access using directional antennas," in *Proc. IEEE Int. Conf. Commun. Workshops (ICC Workshops)*, 2017, pp. 731–736.

[21] G. Liva, "Graph-based analysis and optimization of contention resolution diversity slotted ALOHA," *IEEE Trans. Commun.*, vol. 59, no. 2, pp. 477–487, 2011.

[22] M. Ghanbarinejad and C. Schlegel, "Irregular repetition slotted ALOHA with multiuser detection," in *Proc. 10th Annu. Conf. Wireless On-demand Netw. Syst. Services (WONS)*, 2013, pp. 201–205.

[23] Y.-H. Chiang, Y.-J. Lin, C.-S. Chang, and Y.-W. P. Hong, "Throughput analysis for parallel decoding of irregular repetition slotted ALOHA with noise," *IEEE/ACM Trans. Netw.*, vol. 32, no. 4, pp. 3544–3558, 2024.

[24] S. Alsabbagh, C. Adjih, A. Adouane, and N. Aitsaadi, "Optimization of irregular repetition slotted ALOHA with imperfect SIC in 5G CIoT," in *Proc. IEEE Int. Conf. Commun. (ICC)*, 2025, pp. 5234–5240.

[25] S.-L. Shieh and S.-H. Yang, "Enhanced irregular repetition slotted ALOHA under SIC limitation," *IEEE Trans. Commun.*, vol. 70, no. 4, pp. 2268–2280, 2022.

[26] D. Wang, A. Elzanaty, and M.-S. Alouini, "Age-optimized irregular repetition slotted ALOHA with adaptive coding: Design and analysis," *IEEE Trans. Wireless Commun.*, pp. 1–1, 2025.

[27] F. Clazzer, E. Paolini, I. Mambelli, and Č. Stefanović, "Irregular repetition slotted ALOHA over the Rayleigh block fading channel with capture," in *Proc. IEEE Int. Conf. Commun. (ICC)*, 2017, pp. 1–6.

[28] Y. Takahashi, G. Song, T. Kimura, and J. Cheng, "Irregular repetition slotted ALOHA over Rayleigh block fading channels: Bounds and threshold saturation via spatial coupling," *IEEE Access*, vol. 11, pp. 106 528–106 543, 2023.

[29] D. Jakovetić, D. Bajović, D. Vukobratović, and V. Crnojević, "Co-operative slotted ALOHA for multi-base station systems," *IEEE Trans. Commun.*, vol. 63, no. 4, pp. 1443–1456, 2015.

[30] C.-H. Yu, L. Huang, C.-S. Chang, and D.-S. Lee, "Poisson receivers: A probabilistic framework for analyzing coded random access," *IEEE/ACM Trans. Netw.*, vol. 29, no. 2, pp. 862–875, 2021.

[31] T.-H. Liu, C.-H. Yu, Y.-J. Lin, C.-M. Chang, C.-S. Chang, and D.-S. Lee, "ALOHA receivers: A network calculus approach for analyzing coded multiple access with SIC," *IEEE/ACM Trans. Netw.*, vol. 30, no. 2, pp. 840–854, 2022.

[32] C.-E. Lee, K.-Y. Liao, H.-W. Yu, R. Zhang, C.-S. Chang, and D.-S. Lee, "Convolutional coded poisson receivers," *IEEE Trans. Netw.*, vol. 34, pp. 214–229, 2026.

[33] S. Ogata and K. Ishibashi, "Frameless ALOHA with multiple base stations," in *Proc. 49th Asilomar Conf. Signals, Syst. Comput.*, 2015, pp. 47–51.

[34] S. Ogata, K. Ishibashi, and G. Abreu, "Multi-access diversity gain via multiple base station cooperation in frameless ALOHA," in *Proc. IEEE 18th Int. Workshop Signal Process. Adv. Wireless Commun. (SPAWC)*, 2017, pp. 1–5.

[35] S. Ogata, K. Ishibashi, and G. T. de Abreu, "Optimized frameless ALOHA for cooperative base stations with overlapped coverage areas," *IEEE Trans. Wireless Commun.*, vol. 17, no. 11, pp. 7486–7499, 2018.

[36] C. R. Srivatsa and C. R. Murthy, "On the impact of channel estimation

on the design and analysis of IRSA based systems," *IEEE Trans. Signal Process.*, vol. 70, pp. 4186–4200, 2022.

[37] C. R. Srivatsa and C. R. Murthy, "User activity detection for irregular repetition slotted ALOHA based MMTC," *IEEE Trans. Signal Process.*, vol. 70, pp. 3616–3631, 2022.

[38] G. Song, K. Cai, Y. Chi, and J. Cheng, "Throughput analysis of interference cancellation-based random access with feedback," *IEEE Commun. Lett.*, vol. 22, no. 12, pp. 2423–2426, 2018.

[39] Z. Zhang, Y. Li, G. Song, C. Yuen, and Y. L. Guan, "Random NOMA with cross-slot successive interference cancelation packet recovery," *IEEE Wireless Commun. Lett.*, vol. 9, no. 7, pp. 1065–1069, 2020.

[40] A. Mengali, R. De Gaudenzi, and P.-D. Arapoglou, "Enhancing the physical layer of contention resolution diversity slotted ALOHA," *IEEE Trans. Commun.*, vol. 65, no. 10, pp. 4295–4308, 2017.

[41] A. Mengali, R. De Gaudenzi, and Č. Stefanović, "On the modeling and performance assessment of random access with SIC," *IEEE J. Sel. Areas Commun.*, vol. 36, no. 2, pp. 292–303, 2018.

[42] S. Atapattu, C. Tellambura, and H. Jiang, "A mixture gamma distribution to model the SNR of wireless channels," *IEEE Trans. Wireless Commun.*, vol. 10, no. 12, pp. 4193–4203, 2011.

[43] I. S. Gradshteyn and I. M. Ryzhik, *Table of Integrals, Series, and Products*, 7th ed. San Diego, CA, USA: Academic Press, 2007.

[44] M. K. Simon and M. S. Alouini, *Digital Communication over Fading Channels*, 2nd ed. Hoboken, NJ, USA: Wiley, 2005.

[45] M.-S. Alouini and A. Goldsmith, "Area spectral efficiency of cellular mobile radio systems," *IEEE Trans. Veh. Technol.*, vol. 48, no. 4, pp. 1047–1066, 1999.

[46] P. Bithas, N. Sagias, P. Mathiopoulos, G. Karagiannidis, and A. Rontogiannis, "On the performance analysis of digital communications over generalized-k fading channels," *IEEE Commun. Lett.*, vol. 10, no. 5, pp. 353–355, 2006.

[47] D. B. Da Costa and M. D. Yacoub, "Average channel capacity for generalized fading scenarios," *IEEE Commun. Lett.*, vol. 11, no. 12, pp. 949–951, 2007.

[48] N. P. Le, L. C. Tran, X. Huang, J. Choi, E. Dutkiewicz, S. L. Phung, and A. Bouzerdoum, "Performance analysis of uplink NOMA systems with hardware impairments and delay constraints over composite fading channels," *IEEE Trans. Veh. Technol.*, vol. 70, no. 7, pp. 6881–6897, 2021.

[49] T. M. Cover and J. A. Thomas, *Elements of Information Theory (Wiley Series in Telecommunications and Signal Processing)*. Hoboken, NJ, USA: Wiley-Interscience, 2006.

[50] D. Fukui, Y. Takahashi, G. Song, T. Kimura, Z. Liu, and J. Cheng, "Throughput analysis of SIC-based two-device slotted ALOHA with feedback over Nakagami-m fading channels," in *Proc. Int. Symp. Inf. Theory Appl. (ISITA)*, 2024, pp. 131–136.

[51] J. G. Proakis and M. Salehi, *Digital communications*. McGraw-hill New York, 2001, vol. 4.

[52] S. M. Ross, *A First Course in Probability*, 6th ed. Upper Saddle River, NJ, USA: Prentice Hall, 1998.

[53] Č. Stefanović, E. Paolini, and G. Liva, "Asymptotic performance of coded slotted ALOHA with multipacket reception," *IEEE Commun. Lett.*, vol. 22, no. 1, pp. 105–108, 2018.

[54] Z. Chen, Y. Feng, C. Feng, L. Liang, Y. Jia, and T. Q. S. Quek, "Analytic distribution design for irregular repetition slotted ALOHA with multipacket reception," *IEEE Trans. Veh. Technol.*, vol. 72, no. 1, pp. 1360–1365, 2023.

[55] P. T. Boggs and J. W. Tolle, "Sequential quadratic programming," *Acta Numer.*, vol. 4, pp. 1–51, 1995.